Earth Systems and Environment
https://doi.org/10.1007/s41748-026-01060-3

ORIGINAL ARTICLE

High- and Low-Temperature Hydrogeochemical Processes and their Control on Water Composition in the Domuyo Geothermal System

Esteban Villalba[1] · María F. Lajoinie[2] · Silvina C. Carretero[1] · Rebecca Biagi[3] · Franco Tassi[3]

Received: 8 October 2025 / Revised: 11 January 2026 / Accepted: 28 January 2026

Abstract

In geothermal mountain settings, water-rock interactions critically shape vital water resources. The aim of this study was to characterize water composition, identify the dominant geochemical processes, and constrain mixing relationships between meteoric and geothermal fluids in the Domuyo Geothermal System (Patagonia, Argentina). To achieve this, we present the first integrated hydrogeochemical and mineralogical evaluation of the system, combining water chemistry with the mineralogy of host rocks and hydrothermal precipitates to resolve the processes controlling water composition in this understudied Andean geothermal setting. Water samples from streams, thermal springs, and wet meadows were analyzed together with igneous host rocks and hydrothermal precipitates. Results reveal a marked contrast: upstream waters are cold Ca/Mg-HCO_3 type with low electrical conductivity (~366 µS/cm), whereas thermal springs are Na-Cl type, characterized by high electrical conductivity (~6,106 µS/cm) and elevated silica (~226 mg/L) and SO_4^{2-} (~73 mg/L) concentrations, indicating deep, high-temperature water-rock interaction and magmatic gas input. Downstream samples show intermediate compositions, indicating variable degrees of mixing processes (electrical conductivity ~2,538 µS/cm). Mineralogical analyses document extensive hydrothermal alteration of host rocks (clays, zeolites, iron oxides), while carbonate travertines record CO_2-driven precipitation processes. The integration of hydrochemical data with alteration and secondary mineral assemblages allows reconstruction of water types and mixing proportions and clarifies the geochemical controls that govern fluid evolution in the system. These findings demonstrate the direct impact of geothermal processes on surface water and provide a critical baseline for sustainable water resources management in vulnerable regions where meteoric and geothermal systems interact.

✉ Esteban Villalba
evillalba@gsuite.fcnym.unlp.edu.ar

[1] Centro de Estudios Integrales de la Dinámica Exógena (CEIDE), Facultad de Ciencias Naturales y Museo, Universidad Nacional de La Plata (FCNyM, UNLP), Consejo Nacional de Investigaciones Científicas y Técnicas (CONICET), Calle 64 #3, Ground floor, La Plata, Argentina

[2] Instituto de Recursos Minerales (INREMI), Facultad de Ciencias Naturales y Museo, Universidad Nacional de La Plata (FCNyM, UNLP), Consejo Nacional de Investigaciones Científicas y Técnicas (CONICET), Calle 64 #3, First floor, La Plata, Argentina

[3] Dipartimento di Scienze della Terra (DST), Università di Firenze (UNIFI), Instituto di Geoscienze e Georisorse (IGG), Consiglio Nazionale delle Ricerche (CNR), Via La Pira #4, Firenze, Italia

Published online: 17 February 2026

Graphical Abstract

This graphical abstract provides a comprehensive visual summary of the hydrogeochemical processes governing water composition in the Domuyo Geothermal System (Patagonia, Argentina). It integrates field observations, laboratory analyses, and conceptual modeling to illustrate how water-rock interaction, magmatic inputs, and tectonic controls shape the system's geochemistry. The upper panel presents the data source, with a map of the study area highlighting sampling locations for waters (upstream, downstream, thermal springs) and rocks. Adjacent panels show representative outcrops and rock samples (Varvarco Granodiorite, Upper/Lower Volcanic Cycle) and hydrothermal precipitates (travertine), alongside XRD determinations confirming their mineralogy. The central panel displays the water analyses. Bivariate plots reveal key relationships (Na^+ vs. Cl^-, Na^+ vs. $HCO3^-$, Na^++K^+ vs. $H4SiO4$+$HCO3^-$) that identify dominant processes like base exchange and silicate weathering. The Piper diagram classifies the hydrochemical facies, showing the evolution from Ca-HCO3 upstream to Na-Cl in thermal springs. The lower panel presents hydrogeochemical conceptual models for different sectors. For the upstream area, it depicts plagioclase and alkali feldspar dissolution in streams/rivers and wet meadows. For thermal springs, it illustrates deep circulation, magmatic gas input, sedimentary rock dissolution, and atmospheric gas dissolution, leading to high-temperature fluid discharge. For the downstream area, it shows mixing between geothermal and meteoric waters, with continued base exchange and precipitation in wet meadows and streams. Overall, this visual summary highlights the interplay between deep geothermal processes and shallow surface interactions, controlled by the regional tectonics, which ultimately determine the water composition in this mountainous environment.

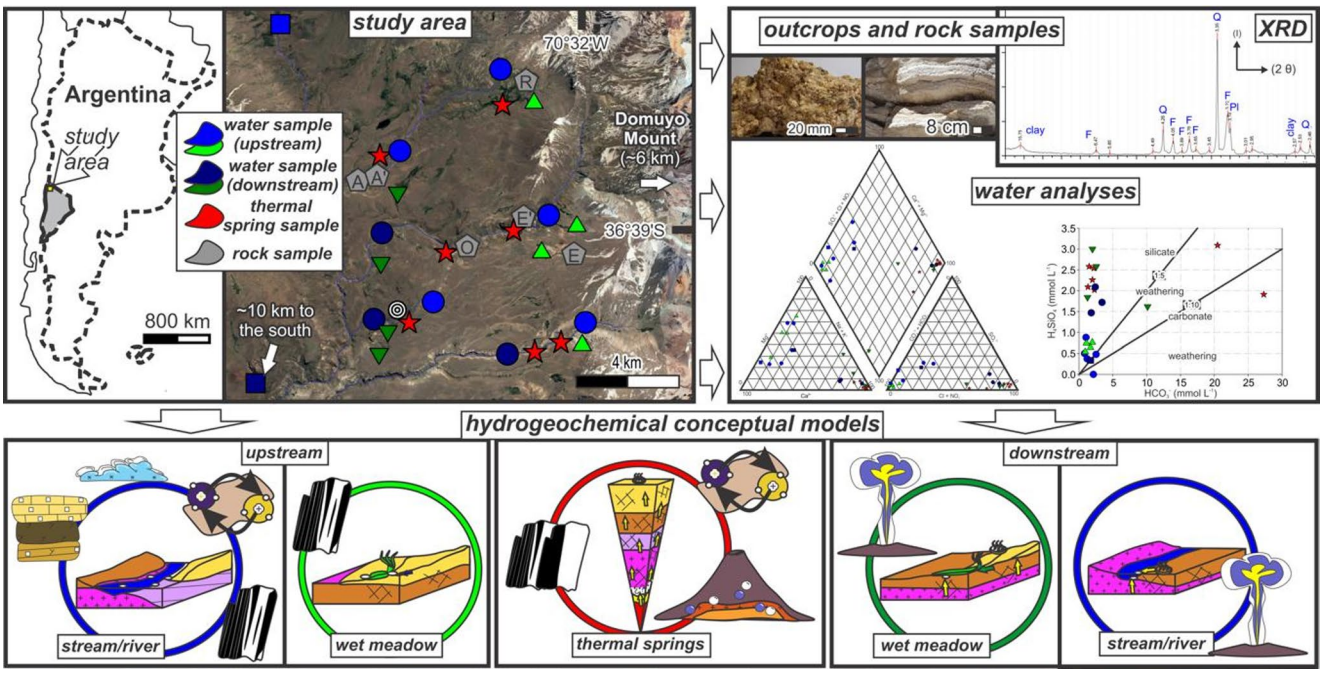

Highlights

- Mixing and water-rock interaction control water composition in the DGS.
- Thermal springs show Na-Cl facies reflecting deep geothermal processes.
- Calcite (travertine) dominates hydrothermal precipitates due to CO_2 degassing.
- Igneous rock dissolution provides major ions to the geothermal fluid.
- New models link deep and surface hydrogeochemical processes determining water chemistry.

Keywords Geochemical processes · Mountain hydrochemistry · Weathering and alteration · Argentinean patagonia

1 Introduction

Water resources are essential for sustaining life and enabling the socioeconomic development of populations. However, in many regions worldwide, water availability for human use is increasingly threatened by climate change, overexploitation, and contamination (Alao 2023; Alao et al. 2024a;

Alao 2025a; Rodell et al. 2018; Scanlon et al. 2023; Taucare et al. 2024). Furthermore, water quality in tectonically active regions, such as volcanic zones, can be affected by the presence of thermal springs (e.g., Benmarce et al. 2023; Chalise et al. 2023). In these settings, geothermal systems represent a significant factor influencing water composition, as they introduce high-temperature fluids and magmatic volatiles into the hydrological cycle through complex water-rock interactions (Giggenbach 1996; Ingebritsen and Manning 1999). Geothermal systems are classified based on their enthalpy and associated temperature. Low-enthalpy systems typically involve fluid temperatures below 150 °C and are often associated with shallow circulation heated by the geothermal gradient (e.g., Lee 2001). Medium- to high-enthalpy systems, characterized by temperatures exceeding 150 °C, usually involve deeper circulation and are often related to recent magmatic activity or convective processes in tectonically active regions (e.g., Eichelberger 2020; Reinoso Carbonell et al. 2025). These systems can significantly impact local hydrogeochemical properties through intense water-rock interaction at elevated temperatures, dissolution of magmatic gases, and the potential for secondary mineral precipitation upon fluid discharge and cooling (Arnórsson et al. 2007; Fournier 1999).

The Southern Volcanic Zone of the Andes (33° and 46° S) encompassing parts of Chile and Argentina, host numerous active potentially active geothermal systems associated with intense tectonic deformation and high magmatic activity (Benavente et al. 2016; Hervé et al. 1984; López-Escobar et al. 1995; Rivas et al. 2024; Robidoux et al. 2025; Tardani et al. 2021; Wrage et al. 2017). These systems offer unique opportunities to study hydrogeochemical processes under conditions of high heat flow, complex lithology, and active tectonics. However, research on the detailed hydrogeochemical evolution within these systems, particularly focusing on the interplay between high- and low-temperature water-rock interactions, magmatic inputs, and hydrothermal precipitation, remains relatively limited compared to systems in other regions (e.g., the western USA, New Zealand, Iceland; Dobson et al. 2004; Reyes and Trompetter 2012; Stefánsson et al. 2019).

The Domuyo system in Argentina Patagonia is representative of such systems. The area is characterized by the coexistence and interaction of (i) a shallow, cold hydrological system, represented by streams and wet meadows located both in steep headwater areas and in the lower basin, where they develop over large mass-wasting deposits with low slopes (Villalba 2023); (ii) a deep, hot geothermal system (e.g., Villalba et al. 2025), the latter evidenced by surface manifestations such as geysers, fumaroles, bubbling pools, among others, which are particularly concentrated on the western flank of Domuyo Mount (e.g., Chiodini et al. 2014); and (iii) host rocks and lithogeological units underground or on the surface which water circulates. Previous studies have documented its geothermal activity, including high-temperature thermal springs (temperature > 90° C; e.g., Chiodini et al. 2014), fumarolic emissions (Tassi et al. 2016), and the mobility of trace elements (Llano et al. 2025; Villalba et al. 2022). Geochemical and isotopic evidence suggest a significant magmatic component influencing the geothermal fluids (Chiodini et al. 2014; Tassi et al. 2016). However, despite these advances, a comprehensive assessment integrating the mineralogical composition of host rocks and hydrothermal precipitates with fluid geochemistry has not been fully undertaken. This represents a significant research gap, as the dominant hydrogeochemical mechanisms controlling water composition across the entire system remain partially understood.

To address this gap, the aim of this study is to identify and improve the understanding of hydrogeological systems in mountainous environments associated with geothermal activity, in order to elucidate the mechanisms that may affect water composition, an increasingly scarce and highly valued resource for local communities. To this end, the hydrogeochemical processes governing water-rock interactions in the surroundings of Domuyo Mount (Argentine Patagonia) were assessed, providing a comprehensive hydrogeochemical model was proposed for a region with scarce knowledge on this topic.

2 Study Area

2.1 Geological Setting

The study area is located within the Southern Volcanic Zone, which is characterized by widespread tectonic deformation and high magmatic activity located mainly on siliceous continental crust (Ramos 1978; Stern 2004). This zone hosts numerous active stratovolcanoes, most of which originated during the late Cenozoic (Ramos 1999). At the latitude of the study area (~36° 38' S) and towards the south, the volcanic arc is characterized by a greater crustal influence and rocks of andesitic, basaltic, and dacitic composition, possibly associated with effusive centers controlled by the structures linked to the development of the magmatic arc (Daniele et al. 2020; Hervé et al. 1984; López-Escobar et al. 1995). Specifically, Domuyo Mount is located in the geological province defined as the Cordillera Principal (Ramos 1999) and presents lithostratigraphic units whose characteristics, distribution and ages were described mainly based on the work carried out by Zanettini et al. (2001) and Narciso et al. (2004), and are summarized below (Fig. 1c).

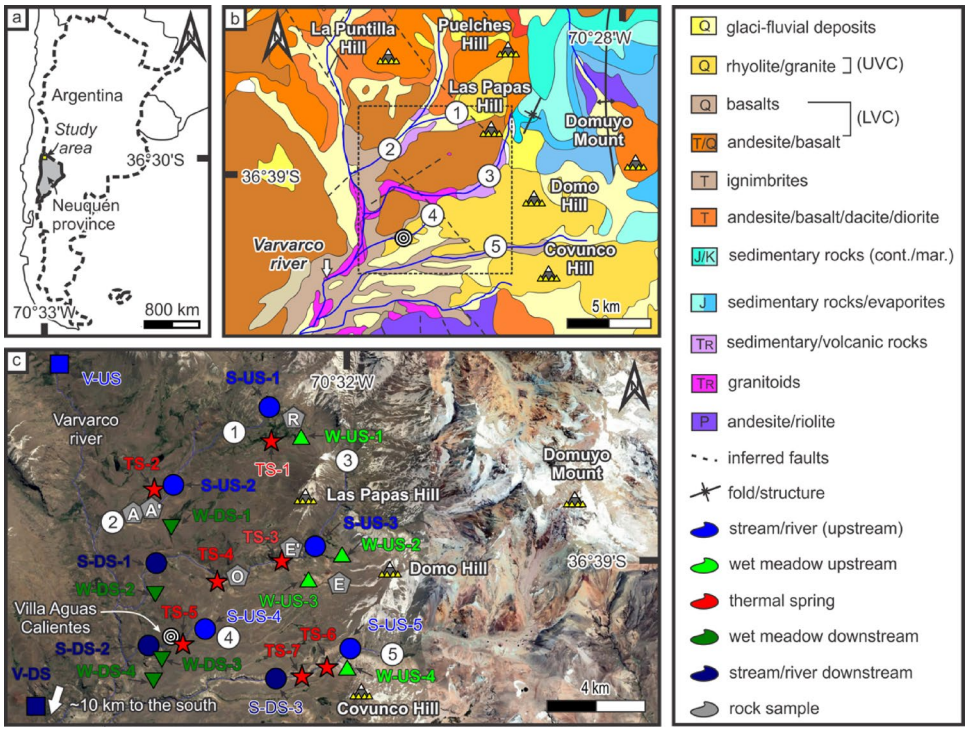

Fig. 1 Regional location of the study area (**a**) and map of the geology (**b**) based on Narciso et al. (2004) and Zanettini et al. (2001). Satellite image of the Domuyo Mount is also presented with water and rock sampling points (**c**). Numbers in (**b**) and (**c**) are Las Papas (1), Ailinco (2), Manchana Covunco (3), Aguas Calientes (4), and Covunco (5) streams, respectively. The letters inside the reference boxes indicate the estimated age of the unit: Quaternary (Q), Tertiary (T), Cretaceous (K), Jurassic (J), Triassic (TR), Permian (P), and Paleozoic age (Pz). Cont.: continental origin, mar.: marine origin

The lithostratigraphic units are composed from base to top by: (i) Permian calc-alkaline volcanic rocks, differentiated into a lower mesosilicic andesitic series and an upper silicic rhyolitic series (Llambías and Stipanicic 2002); (ii) Triassic granitoids that include granodiorites and tonalites with abundant amphiboles and whose most obvious representation in the study area is the Varvarco Granodiorite (Pesce 1981); (iii) Triassic sedimentary rocks and volcanic rocks represented by conglomerates, pelites, sandstones, and tuffs interbedded with andesites, dacites, and basalts (Spalletti et al. 1991; Leanza and Hugo 1997); (iv) Jurassic marine sedimentary rocks composed of pelites, marls, sandstones, and stratified gypsum with limestone interlayers (Dellapé et al. 1978; Gulisano et al. 1984; Llambías and Leanza 2005); (v) Jurassic to Triassic continental and marine sedimentary rocks composed of psammo-pelitic, black and calcareous pelites, and bituminous micritic limestones (Kietzmann and Vennari 2013; Leanza 1972; Stipanicic et al. 1968); (vi) Tertiary volcanic rocks composed of lava flows, tuffs, volcanic agglomerates, porphyritic andesites and andesitic to dacitic tuffs, and diorites (Rapela and Llambías 1985); (vii) loosely packed Tertiary pyroclastic rocks and volcanic agglomerates, of dacitic to andesitic composition (Llambías et al. 1978); (viii) volcanic rocks comprising andesites, basandesites and pyroclastic rocks described as Lower Volcanic Cycle (LVC); (ix) volcanic and plutonic rocks represented by rhyolites, granites, phreatomagmatic deposits, volcanic breccias and rhyolitic to dacitic lavas defined as Upper Volcanic Cycle (UVC) (Brousse and Pesce 1982; Japan International Cooperation Agency –JICA– 1983); finally, the sequence of units culminates in a cover of extensive glacifluvial deposits (Fig. 1c). Significantly, recent studies link the UVC to a shallow magmatic chamber, which acts as the heat source driving the current geothermal anomalies (Silva-Fragoso et al. 2021).

2.2 Hydrological Setting

The hydrological system of the Domuyo region is governed by a semi-arid climate, with an annual precipitation of 655 mm and mean temperature of 4.6 °C. Climate presents a seasonal variability characterized by a cold and humid period (April-September) and warm and dry period (October-March). Precipitation and snow/ice melt constitute the main recharge sources for surface and groundwater bodies, consistent with regional isotopic models that identify meteoric water as the primary origin for Andean hydrothermal systems (Panarello et al. 1992; Villalba 2023; Villalba et al. 2025).

The surface water network consists of intermontane water courses (Fig. 1b, c) originating in the high Andes. These streams flow through the landscape, exhibiting significant chemical changes along their course, which indicate geochemical processes involved (Villalba et al. 2022). Notably, some water courses sections act as gaining streams, receiving contributions from groundwater discharge points, including wet meadows and thermal springs (Villalba 2023). Conversely, areas with abundant alluvial/colluvial deposits

can act as losing streams (Villalba et al. 2025). Groundwater flow is largely controlled by the complex fractured geology typical of the Andean Precordillera. Localized aquifers are inferred to exist within fractured igneous rocks and more permeable sedimentary units (e.g.Alao et al. 2023, 2024b, 2025b; Alao and Abubakar 2025; Villalba et al. 2025). Discrete discharge occurs focally as cold springs and is prominently manifested through the extensive Domuyo Geothermal System, where thermal springs contribute significantly to the hydrological and hydrochemical budget of the area (Chiodini et al. 2014; Tassi et al. 2016; Villalba et al. 2022). The interaction between these distinct hydrological components (meteoric surface/groundwater and deep geothermal fluids) results in a highly heterogeneous and seasonally dynamic water resource system. Understanding this interplay is crucial for the sustainable management of these scarce and vulnerable freshwater sources in the Domuyo Geothermal System and its surroundings, which are critical for local ecosystems and rural communities that depend on them for human consumption, agricultural irrigation, and livestock activities (Villalba 2023).

3 Methodology

A comprehensive methodology was designed integrating field surveys, laboratory analysis, and spatial data integration. The approach combined the characterization of geological materials with detailed water sampling and physicochemical analysis, aiming to establish relationships between lithology, mineral precipitation, and water composition.

3.1 Geological and Hydrological Characterization

The general geological and litho-geomorphological framework of the study area was established through the analysis of existing geological maps, bibliographic data, and the interpretation of high-resolution satellite imagery (Google Earth Pro, Bing Maps). Field surveys were conducted between November 5 and 15, 2018, using geopositioned points recorded with a high-sensitivity GPS device (Garmin eTrex®) to identify and map geothermal manifestations, lithological boundaries, and sampling sites. Representative field photographs of the different lithostratigraphic units were taken to illustrate the landscape and geological context.

Table 1 Names and location of the lithostratigraphic units collected in the study area

Sample	Lithostratigraphic unit	Location
R	Upper Volcanic Cycle	Rincón de las Papas
E	Upper Volcanic Cycle	El Humazo
E’	Upper Volcanic Cycle	El Humazo
A	Lower Volcanic Cycle	Ailinco
A’	Lower Volcanic Cycle	Ailinco
O	Varvarco Granodiorite	Las Olletas

3.2 Rock and Salt Samples

The analysis of rock and salt samples is intended to provide insights into the mineralogical controls on water composition. The rock sampling strategy was designed based on the lithological heterogeneities in areas of active geothermal manifestations and potential water-rock interaction (Fig. 1c). Six igneous rock samples were collected: three corresponding to the UVC (samples R, E, E’), two to the LVC (samples A, A’), and one of the Varvarco Granodiorite (sample O) (Table 1). These units were selected based on their proximity to geothermal manifestations and their potential to influence groundwater chemistry through weathering and hydrothermal alteration processes. In addition, samples of salts deposited by precipitation from hydrothermal fluids were collected in the same sampling areas to assess secondary mineral formation. Rock samples were macroscopically described in the field, and the precipitated salts were tested for effervescence using concentrated hydrochloric acid (3 mol L^{-1}) to confirm the presence of carbonates. Subsequently, in the mesoscopy laboratory of the Institute of Mineral Resources (INREMI-CIC-UNLP), the samples were described under a SZH10 binocular magnifier with a magnification ratio of 10:1. A fraction of each sample was crushed, pulverized, and analyzed by X-ray diffraction (XRD). The diffractograms were obtained with a PANalytical X’Pert Pro equipped with a copper lamp ($\lambda = 1.5403$ Å) operating at 40 mA and 40 kV. Readings in the total fraction were made between 5 and 65 ° 2θ and for the clayey fraction the technique of decantation, air drying (2 to 32 ° 2θ), glycol treatment (2 to 30 ° 2θ) and calcination at 550 ° C for 2 h (2 to 15 ° 2θ) was used. The interpretation was performed using PANalytical X’Pert High Score Plus v3.0 software. Petrological classification of pyroclastic rocks followed the scheme proposed by Mazzoni (1986), modified from Teruggi et al. (1978), while volcanic and plutonic rocks were classified according to Streckeisen (1980). The salts were classified as travertines following Pentecost and Viles (1994), or as sinters according to Rodgers et al. (2004).

3.3 Water Samples

A total of 25 water samples were collected from different hydrological settings to characterize the spatial variability of the hydrogeochemical system. The monitoring network was established in three distinct zones: (i) upstream areas

without thermal influence (S-US, W-US, V-US; (ii) areas with active geothermal manifestations (TS); and (iii) downstream areas potentially influenced by thermal discharge (S-DS, W-DS, V-DS) (Table 2; Fig. 1). Physicochemical parameters including pH, temperature (T), and electrical conductivity (EC), were measured in situ using a portable multiparameter probe (Lutron® WA-2017SD). Water aliquots were collected in 1000 ml polyethylene bottles, stored under refrigeration, and analyzed following standardized norms according to American Public Health Association (APHA 1998). Analytical determinations include titration-based measurements of carbonates (CO_3^{2-}), bicarbonates (HCO_3^-), chlorides (Cl^-), calcium (Ca^{2+}) and magnesium (Mg^{2+}); flame photometry (Crudo Caamaño Ionometer sodium) for sodium (Na^+) and potassium (K^+); and UV-Visible spectrophotometry (Shimadzu UV-160 A, double-beam) for sulfates (SO_4^{2-}), nitrates (NO_3^-) and silica (H_4SiO_4). Analytical precision was assessed through duplicate analyses and certified reference standards.

3.4 Data Integration

To evaluate the role of water-rock interactions in controlling water composition, all data were integrated using a Geographic Information System (QGIS). Sample locations (Fig. 1) were plotted on the geological map and satellite image to visualize the spatial distribution of water types and their relationship with lithological units and geothermal manifestations. This allowed for correlation analysis between water chemistry, host rock geology, and proximity to geothermal discharge points. Water type classification diagrams or stoichiometric diagrams were used to interpret hydrogeochemical processes (e.g., Piper 1944). Furthermore, the integrated spatial analysis sustained the hydrogeochemical conceptual models. The mineralogical composition of precipitated salts was compared with the ionic composition of water samples to assess potential links between mineral saturation and salt precipitation in the hydrothermal system.

Table 2 Names of the water samples collected in the study area based on their location in the basin and with respect to sectors with geothermal manifestations

Sample	Type	Sector	Number of samples
V-US	Varvarco river	upstream	1
S-US	stream	upstream	5
W-US	wet meadow	upstream	4
TS	thermal spring	middle basin	7
S-DS	stream	downstream	3
W-DS	wet meadow	downstream	4
V-DS	Varvarco river	downstream	1

4 Results

4.1 Lithological Characteristics of Main Igneous Units

Satellite images combined with field observations enabled the differentiation of lithological units and the identification of rock outcrops associated with each of them. Additionally, significant deposits resulting from gravitational mass movements were recognized, which in many cases obscure or partially bury the primary outcrops, complicating their identification. Despite these limitations, the sequence of igneous rocks, ranging from the crystalline basement to the uppermost volcanic rocks, was identified.

The crystalline basement, represented by the Varvarco Granodiorite, was recognized in the Las Olletas area (sample O, Figs. 1c and 2a and b), where it displays significant weathering and surface oxidation, evidenced by reddish colours, and a crumbly structure. It exhibits a coarse-grained texture and is mainly composed of quartz, plagioclase, alkali feldspar, clays, and micas. Based on its modal composition, the rock was classified as granodiorite (Q ~ 54%; A ~ 15%; P ~ 31%). Overlying the basement are the volcanic rocks of the LVC, recognized in the Ailinco area, where two distinct lithologies were identified: pyroclastic rocks and lava flows (samples A and A', respectively, Figs. 1c and 2c). The pyroclastic rocks are white, grey and brown in colour, and are composed of abundant matrix (M) containing lithoclasts (L) of aphanitic to porphyritic volcanic rocks (comprising oxides, plagioclase, quartz and alkali feldspar), along with crystalloclasts (C) of plagioclase, quartz, amphibole (hornblende), oxides and clays, and classified as lapillite (M ~ 60%; L ~ 30%; C ~ 10%). The lava flows are brown, grey, and yellowish-white, exhibiting aphyric to porphyritic textures; the latter features plagioclase phenocrysts set within an aphanitic groundmass. These rocks also contain alkali feldspars, oxides, clays, and micas, and have been classified as phenoandesite (Q ~ 11%; A ~ 11%; P ~ 78%). The uppermost unit in the lithostratigraphic sequence is the UVC, identified in the Rincón de Las Papas and El Humazo areas (samples R and E, respectively, Fig. 1c). Sample R exhibits a brown to gray-brown coloration, a brecciated structure, and is composed of lithoclasts of vitroporphyritic volcanites, vitroclasts, and crystalloclasts immersed in a glassy matrix (Fig. 2d). The minerals assemblange includes quartz, alkali feldspar, clays, micas, and oxides. The rock was classified as lapillite based on its components (M ~ 92%; L ~ 5%; C ~ 3%). Two samples were collected from El Humazo (E and E'), due to the presence of distinct lithologies recognized in outcrop, and their close spatial association with water sampling sites (Fig. 1). The E sample is light grey to brown in colour, crumbly, and displays a porphyritic texture

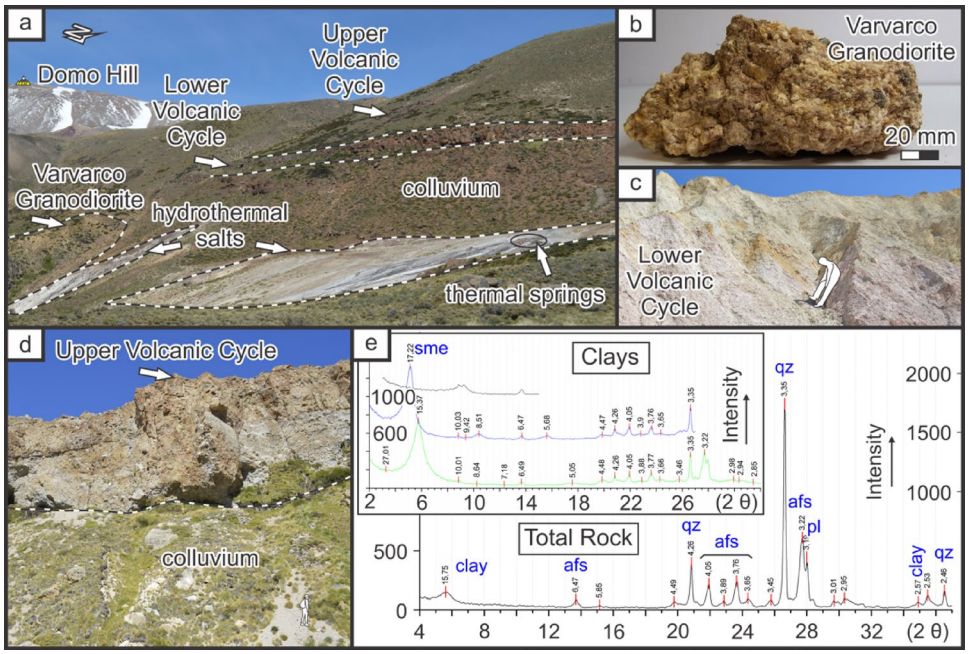

Fig. 2 (**a**) General view of Las Olletas geothermal zone (O) with the representative igneous lithostratigraphic units of the study area marked. (**b**) Photographs of rock hand samples from the crystalline basement. (**c**, **d**) Outcrop of volcanic rocks from LVC and UVC, respectively. (**e**) XRD diffractogram of a volcanic rock from LVR. Quartz (qz); alkali feldspar (afs); plagioclase (pl); smectite (sme)

Table 3 Main characteristics of rock samples from the study area

Sample	O	A	A'	*R*	E	E'
Site	Las Olletas	Ailinco	Ailinco	Rincón de las Papas	El Humazo	El Humazo
Observations	coarse-grained texture, crumbly, reddish colours (oxidation)	clastic to brecciated structure, powdery alteration in surface	aphyric to porphyritic textures, with clays and oxides	brecciated structure, glassy matrix	crumbly, porphyritic texture. Clay presence	clastic to brecciated structure, alteration to clays/zeo
Modal composition[(1)]/ Elements[(2)]	[(1)]Q ~ 54%; A ~ 15%; *P* ~ 31%	[(2)]M ~ 60%; L ~ 30%; C ~ 10%	[(1)]Q ~ 11%; A ~ 11%; *P* ~ 78%	[(2)]M ~ 92%; L ~ 5%; C ~ 3%	[(1)]Q ~ 44%; A ~ 36%; *P* ~ 20%	[(2)]M ~ 64%; L ~ 6%; C ~ 30%
XRD mineralogy	qz pl, afs, clays, crs	qz, pl, afs, clays (sme, ilt), crs, mag	pl, qz, afs, clays (sme), crs, mag	qz, afs, clays (mica, kln)	afs, qz, pl, hbl, crs, trd, clays (sme, kln)	pl, afs, qz, crs, mag, zeo, hbl
Lithology	granodiorite	lapillite	andesite/basalt	lapillite	rhyolite	lapillite
Lithostratigraphic unit	Varvarco Granodiorite	Lower Volcanic Cycle	Lower Volcanic Cycle	Upper Volcanic Cycle	Upper Volcanic Cycle	Upper Volcanic Cycle

Modal composition (Q: quartz; A: alkali feldspar; P: plagioclase) are based on visual estimation with comparative percentage chart. XRD mineralogy indicates phases detected by X-ray diffraction analysis. Mineralogy abbreviations are quartz (qz); plagioclase (pl); alkali feldspar (afs); cristobalite (crs); hornblende (hbl); kaolinite (kln); trydimite (trd); magnetite (mag); smectite (sme); illite (ilt); zeolite (zeo)

with subhedral to anhedral phenocrysts of alkali feldspar, quartz, plagioclase, oxides, and scarce amphibole, embedded in a brown aphanitic groundmass. Clays identified by X-ray include smectite and kaolinite. This rock was classified as phenorhyolite (Q ~ 44%; A ~ 36%; P ~ 20%). The mineralogy of the described rocks at the mesoscopic scale was also verified through XRD determination (Fig. 2e). The E' sample is composed of lithoclasts of porphyric, microporphyric, and aphanitic volcanic rocks, crystalloclasts, and abundant matrix. The global mineralogy of this sample is composed by plagioclase, quartz, a few alkali feldspars, hornblende, and very low proportion of biotite. Sieving and dissolution rims and replacement patches containing zeolites and clays were recognized in plagioclase, as well as sieving textures in amphiboles with opaques boundaries constituting a semi-mantled texture. X-ray diffraction indicated presence of plagioclase, alkali feldspar, quartz, cristobalite, magnetite, zeolites (clinoptilolite/heulandite), and hornblende. The classification of the rock was lapillite (M ~ 64%; L ~ 6%; C ~ 30%).

A summary of the main characteristics of the rock samples, including their site, general observations, modal composition, XRD mineralogy, lithology, and lithostratigraphic unit, is presented in Table 3. This table provides a concise overview of the mineralogical composition and alteration processes affecting the host rocks across the study area.

Additionally, extensive surface coverage was identified, caused by gravitational movements that form hillside

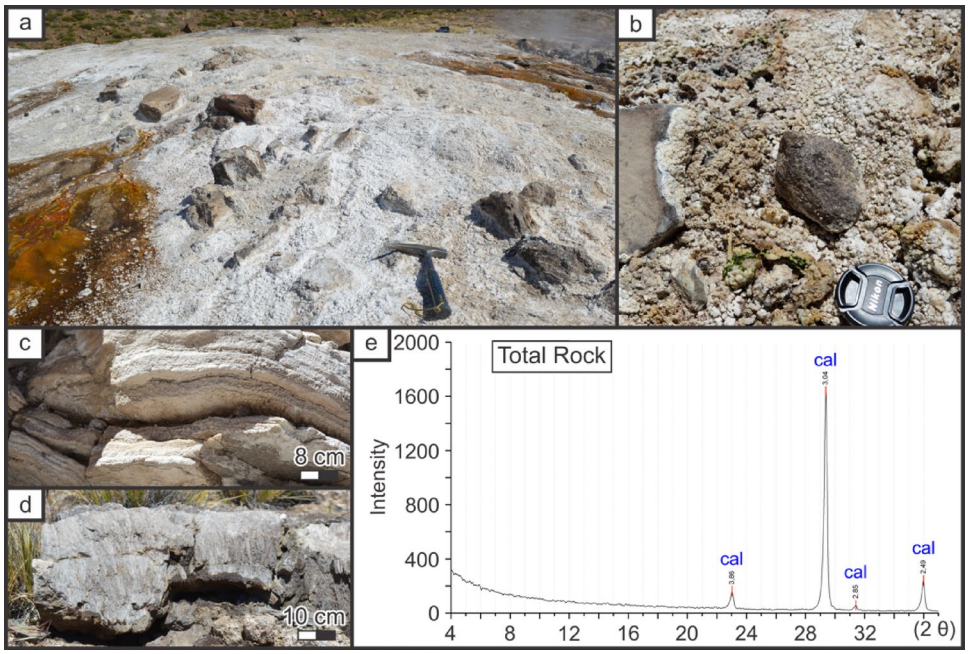

Fig. 3 Outcrop photographs of salt deposits precipitated from hydrothermal fluids. (**a**) Shield-shaped accumulations covering valley slopes in Las Olletas, (**b**) granular to stromatic structures, (**c**) parallel layers structures observed in El Humazo, (**d**) feathery crystal growth in Las Olletas, and (**e**) X-ray diffractogram showing the carbonate composition. Calcite (cal)

deposits and higher-level mass-wasting processes such as landslides and rock avalanches (Villalba et al. 2025).

4.2 Outcrop Characteristics of Salts Derived from Hydrothermal Fluids

In several geothermal areas, salt deposits originating from precipitation from thermal water have been recognized, displaying diverse morphologies, structures, and compositions. Their coloration is usually homogeneous or presents a combination of white, gray, light yellow, brown, and very dark gray tones. The extent of these deposits varies considerably, ranging from 130 m^2 (Ailinco) to approximately 35,000 m^2 (Las Olletas). At the outcrop scale, the deposits form dome-like structures, parallel horizontal packages, or cover valley slopes (Fig. 3a; Las Olletas). The recognized structures include granular, laminar, parallel-layered, stromatic, massive, and mammelonar consolidated material (Fig. 3b, c). Field observations indicate that the vast majority of precipitated salt samples are carbonatic in composition, as evidenced by hexagonal crystalline growth and feathery-like structures (Fig. 3d), along with effervescence reaction upon contact with acid (Fig. 3e). In this regard, X-ray diffraction analyses of these samples confirmed that calcite is the only mineral phase present (Fig. 3f). However, minor outcrops of siliceous material, non-reactive to effervescence, were recognized, with a restricted distribution in a sector of Las Olletas and with curvilinear X-ray diffraction pattern typical of material lacking crystalline structure.

A summary of the features of the salts derived from the hydrothermal fluids observed in the main geothermal zones of the Domuyo Geothermal System, including their areal extent, dominant morphology, recognized structures, field composition, and XRD mineralogy, is presented in Table 4. This table provides a concise overview of the spatial variability in deposit type and composition across the study area.

Table 4 Summary of the key characteristics of salts derived from hydrothermal fluids observed in the main geothermal zones of the Domuyo geothermal system

Feature	Description
Areal Extent	Varies considerably, ranging from ~130 m^2 (Ailinco) to ~35,000 m^2 (Las Olletas).
Dominant Morphology	Shield-shaped accumulations covering valley slopes; dome-like structures; parallel horizontal packages.
Recognized Structures	Granular, laminar, stromatic, feathery crystal growth, mammelonar.
Composition (Field)	Carbonate (effervescence reaction).
XRD Mineralogy	Calcite (travertines); minor amorphous silica (sinters) in some sectors.
Implications	Calcite occurrence indicates CO_2-driven carbonate precipitation as dominant process. Localized siliceous material suggests supersaturation conditions and precipitation of silica in specific sectors.

4.3 Physicochemical Properties and Composition of Waters

Within the study area, three main sectors were delineated based on the spatial distribution of geothermal surface manifestations. These include: (i) a headwater basin sector located upstream of the thermal springs; (ii) a middle basin sector characterized by intense geothermal activity and the

presence of thermal springs; (iii) a lower basin sector located downstream of geothermal manifestations. The analytical results for the studied waters are presented in Table 5.

Samples from the upstream sector (S-US, W-US) exhibit relatively low T (~17° C) and EC (~366 µS cm^{-1} for S-US and 151 µS cm^{-1} for W-US), with pH values ranging between 6.4 and 8.2. The dominant ionic composition is characterized by $HCO_3^- > SO_4^{2-} > Cl^- > NO_3^-$ for anions and $Ca^{2+} > Mg^{2+} > Na^+ > K^+$ for cations (Table 5). The hydrochemical facies is predominantly Ca-HCO_3 type or mixed Ca/Mg-HCO_3 type (Fig. 4).

Thermal spring samples (TS) present high T (~63° C) and EC (~6,106 µS cm^{-1}) conditions, with pH values varying between 5.2 and 8.8 (Table 5). The ionic composition is dominated by $Cl^- > HCO_3^- > SO_4^{2-}$ for anions and $Na^+ > Ca^{2+} > K^+ > Mg^{2+}$ for cations. These waters are characterized by marked Na-Cl facies (Fig. 4), with significantly higher average concentrations of Na^+ (1,237 mg L^{-1}) and Cl^- (1,761 mg L^{-1}) compared to upstream waters (Na^+ and Cl^- from S-US ~ 8.4 and ~ 13.2 mg L^{-1}; Na^+ and Cl^- from W-US ~ 3 and 7.1 mg L^{-1}, respectively).

Downstream samples from streams (S-DS) and wet meadows (W-DS) show intermediate T (S-DS ~ 31° C, W-DS ~ 25° C) and EC values (S-DS ~ 2,538 µS cm^{-1}, W-DS ~ 1,593 µS cm^{-1}) compared to upstream (S-US, W-US) and thermal springs (TS). The pH values are relatively constant (7.2–7.7 for S-DS, 6.4–7.5 for W-DS). The ionic composition is intermediate between thermal and upstream end-members. Anion dominance follows $Cl^- > HCO_3^- > SO_4^{2-}$, and cation dominance follows $Na^+ > Ca^{2+} > K^+ > Mg^{2+}$, resulting in Na-Cl facies for both S-DS and W-DS (Fig. 4). Average concentrations of Na^+ (S-DS ~ 338 mg L^{-1}; W-DS ~ 315 mg L^{-1}) and Cl^- (S-DS ~ 580 mg L^{-1}; W-DS ~ 372 mg L^{-1}) are significantly higher than upstream values but lower than TS.

The V-US sample exhibited relatively low T (19° C), low EC (121 µS cm^{-1}), and a Ca-HCO_3 hydrochemical facies (Fig. 4), with Ca^{2+} and HCO_3^- concentrations of 30 mg L^{-1} and 103 mg L^{-1}, respectively. The V-DS sample, showed a lower T (15° C), increased EC (245 µS cm^{-1}), and a shift in hydrochemical facies towards Ca/Mg-HCO_3 type (Fig. 4), with Ca^{2+} (19 mg L^{-1}), Mg^{2+} (10 mg L^{-1}), and HCO_3^- (97 mg L^{-1}) as main constituents.

In addition to the major ions, dissolved silica concentrations, expressed as H_4SiO_4, varied significantly among sample groups (Table 5), following the sequence: S-US (~43 mg L^{-1}) < W-US (~65 mg L^{-1}) < S-DS (~169 mg L^{-1}) < W-DS (~218 mg L^{-1}) < TS (~226 mg L^{-1}).

5 Discussion

The hydrogeochemical evolution of waters in the Domuyo Geothermal System is governed by a complex interplay of processes, including high-temperature water-rock interaction, magmatic gas input, secondary mineral precipitation, cation exchange, and mixing between geothermal and meteoric waters. These processes are spatially and chemically linked, shaping the chemical signature across the system.

5.1 Hydrothermal Alteration

The interaction between geothermal fluids and host rocks results in extensive hydrothermal alteration, producing secondary minerals (e.g., clays and zeolites), as evidenced by petrologic observations and XRD analysis (Table 3). Two main types of hydrothermal expression were identified: (i) primary rocks that have undergone geothermal alteration, and (ii) surface precipitates formed from ascending hydrothermal fluids. These processes are not isolated phenomena; they form a continuous geochemical pathway that shapes the final water composition.

One of the key mechanisms of hydrothermal alteration is mineral dissolution, a process virtually ubiquitous in geothermal discharges. This is evidenced by sieving textures in phenocrysts and crystalloclasts of plagioclase and amphibole, as well as the presence of "ghost minerals" which indicate partial dissolution and pseudomorphic replacement (e.g., Holdren and Berner 1979). Neoformation of minerals was also observed, mainly from the zeolite group, as found in El Humazo site. Devitrification was identified by the presence of spherulites and axiolitic textures within a felsic matrix, which gave rise to a textural reorganization to crystalline elements (e.g., Marshall 1961) in Rincón de Las Papas. These microstructural changes are particularly significant for water chemistry, as they enhance the release of alkali ions (Na^+ and K^+) into the solution. This process provides the source ions necessary for the base exchange mechanisms discussed in Sect. 5.2.2. Oxidation-reduction processes are indicated by the widespread presence of secondary iron oxides (e.g., magnetite in XRD analysis, Table 3), affecting the primary rock matrix. These phases, which replace primary minerals or fill fractures, reflect the interaction with oxidizing fluids. This mechanism is further evidenced by the presence of coronas around amphibole and by colour changes of primary minerals, often accompanied by secondary opaque minerals formation, features notably observed at El Humazo, although present across most geothermal discharge zones. This mineralogical evidence is consistent with the mixing of deep reducing geothermal fluids and oxygenated meteoric waters near the surface, increasing the redox potential and promoting the

Table 5 Physicochemical parameters, ionic and silica content of water samples of the study area

Sample	pH	T	EC	CO_3^{2-}	HCO_3^-	Cl^-	SO_4^{2-}	NO_3^-	Ca^{2+}	Mg^{2+}	Na^+	K^+	H_4SiO_4
	dimensionless	° C	µS cm^{1-}	mg L^{1-}									
V-US	7.1	19	121	0	103	0.3	16	0.6	30	5.9	1.8	0.9	33
S-US-1	6.6	13	567	0	63	0.2	2.0	0.6	11	2.7	4.5	1.4	85
S-US-2	7.0	16	39	0	73	0.7	1.5	1.4	8.8	9.1	1.8	0.5	36
S-US-3	8.2	18	649	0	154	41	52	0.9	69	14	13	4.8	46
S-US-4	7.7	21	117	0	50	3.1	3.4	4.3	5.3	6.4	2.5	1.4	49
S-US-5	7.3	16	456	0	130	21	39	0.7	34	17	20	2.6	0
W-US-1	6.4	23	92	0	120	2.0	2.8	1.4	15	11	5.1	0.5	73
W-US-2	7.3	15	137	0	103	2.4	1.3	1.6	19	13	3.3	0.0	62
W-US-3	7.5	19	330	0	56	2.3	2.7	1.7	4.4	7.0	2.0	1.0	52
W-US-4	7.3	12	45	0	66	0.4	0.6	1.2	9.7	2.7	1.6	0.0	72
TS-1	5.2	36	8,100	0	1,249	2,387	31	0.5	180	74	1,860	130	297
TS-2	6.2	25	7,080	0	1,665	1,648	24	2.8	52	57	1,260	37	183
TS-3	8.8	90	6,690	39	121	1,855	105	0.0	21	11	1,360	90	218
TS-4	6.6	83	1,480	0	133	1,565	52	0.9	35	2.7	1,040	69	244
TS-5	8.7	70	3,880	0	138	937	69	1.5	17	9.8	640	51	195
TS-6	8.0	80	8,450	24	91	2,285	119	0.7	32	7.5	1,480	160	248
TS-7	7.7	59	7,060	53	81	1,648	109	1.0	41	16	1,020	86	201
S-DS-1	7.5	29	2,330	11	146	471	53	0.7	61	14	244	42	201
S-DS-2	7.2	40	3,990	0	207	965	56	1.0	22	15	610	52	165
S-DS-3	7.7	24	1,295	0	110	305	75	0.6	37	10	159	18	141
V-DS	7.6	15	245	0	97	15	23	0	19	9.6	12	2.1	34
W-DS-1	6.4	24	640	0	617	3.0	13	2.7	13	18	200	2.0	156
W-DS-2	7.0	19	440	0	76	72	7.1	2.5	3.5	13	50	6.2	177
W-DS-3	6.8	26	1,910	0	121	525	17	1.5	11	6.4	400	25	289
W-DS-4	7.5	29	3,380	0	155	888	33	2.2	13	12	610	52	248

The samples were grouped according to their type and spatial position (from north to south and from upstream to downstream). S-US: upstream samples; S-DS: downstream samples; W-US: upstream wet meadows samples; W-DS: downstream wet meadows samples; TS: thermal springs; V-US: upstream Varvarco river sample; V-DS: downstream Varvarco river sample

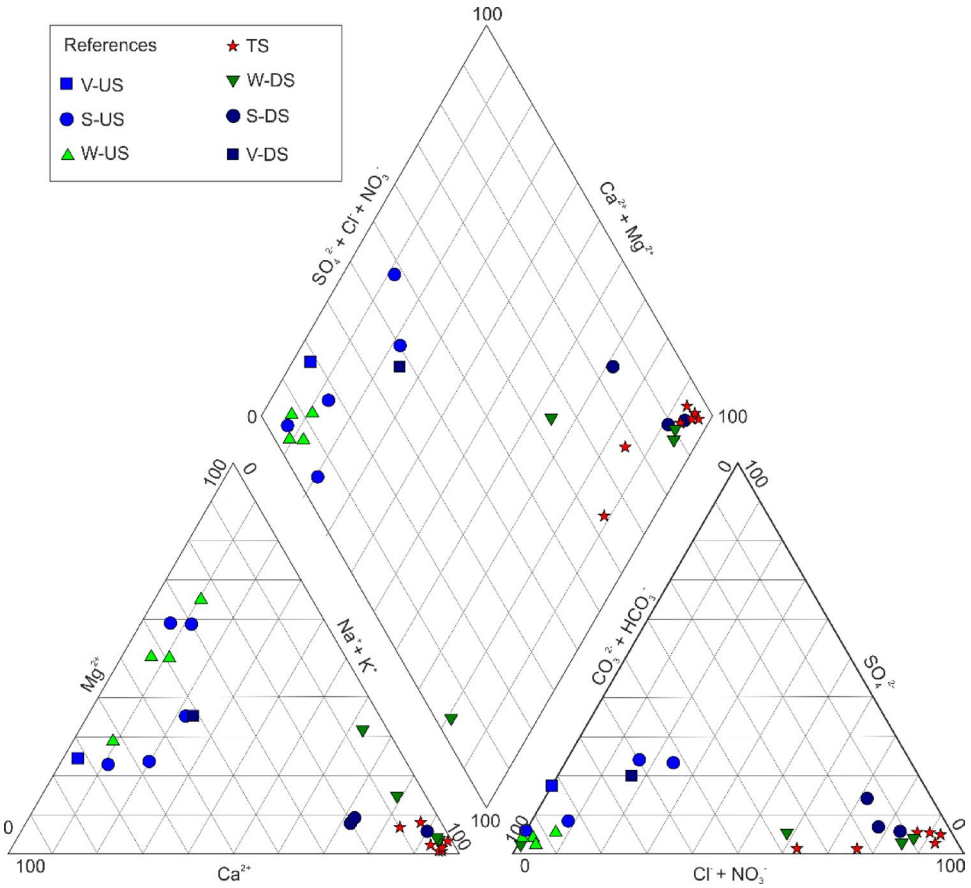

Fig. 4 Piper (1944) diagram presenting the distribution of major ion in the different water samples from the study area

precipitation of Fe-oxides (e.g., Hem and Cropper 1962). This hydrogeochemical control is quantitatively corroborated by contrasting the fluid chemistry with the solid phase composition. While dissolved iron in the TS shows a very low relative mobility (RM < 1; Llano et al. 2025) indicating its removal from solution, the associated precipitates exhibit high Fe concentrations (400 − 16,000 ppm; Villalba et al. 2020). These reddish-brown deposits, rich in iron oxides and hydroxides, act as efficient sinks not only for iron but also for trace elements like arsenic, which is adsorbed onto these mineral phases (Villalba et al. 2020). Thus, the field observation of widespread iron coatings is geochemically consistent with the efficient oxidative precipitation occurring at the discharge zones. Additionally, discoloration was also observed in outcrops in the field, resulting in "washed-out" colors or bleaching appearances, as reported in Ailinco and El Humazo (D'Elia et al. 2020; Mas et al. 2000). Finally, hydration processes were indicated by the presence of limonite minerals and a crumbly structure in the field, which can be described by the reaction: hematite + H_2O ↔ limonite (Palacios et al. 2011). These features were primary identified in Ailinco and Las Olletas.

On the surface, rocks with signs of alteration reveal deeper processes associated with water-rock interaction. These pervasive alteration processes fundamentally modify the rock matrix, generating reactive surfaces and secondary minerals (e.g., clays, zeolites observed in El Humazo) that subsequently play a crucial role in cation exchange reactions (see Sect. 5.2.2).

The second major hydrothermal expression is the formation of secondary mineral deposits on the surface which reflects the distinct physicochemical conditions governing fluid discharge and cooling, providing evidence of the underlaying geothermal system dynamics. The formation of travertine deposits, composed of calcite (Sect. 4.2, Table 4), reflects the supersaturation of CO_2-rich thermal waters with respect to $CaCO_3$ upon discharge and cooling. The decrease in CO_2 partial pressure and temperature shifts the equilibrium of the reaction: $Ca^{2+} + 2HCO_3^- \rightarrow CaCO_{3(s)} + CO_{2(g)} + H_2O$, leading to calcite precipitation (e.g., Fouke et al. 2000; Pentecost 2005). The dominance of calcite over other carbonate phases (e.g., aragonite, dolomite) suggests precipitation under moderate temperature and alkaline conditions, characteristic of shallow discharge zones (Capezzuoli et al. 2014; Kele et al. 2015). This process is kinetically favored under the moderate temperature and alkaline conditions prevalent during surface discharge, consistent with the high HCO_3^- concentrations observed in TS and the widespread calcium depletion relative to anions (e.g., Kele et al. 2015). The spatial distribution of travertines therefore

marks outflow zones where mixed or cooled geothermal fluids release CO_2, as suggested by the fumarolic compositions (Tassi et al. 2016). The textures and structures of these deposits described directly reflect the dynamic conditions of flow rate, temperature, and saturation at the time of deposition (e.g., rhythmicity of deposition) (Pentecost and Viles 1994; Capezzuoli et al. 2014).

In contrast, siliceous sinters represent the precipitation of amorphous silica (e.g., opal-A, chalcedony) from highly saturated, high-temperature geothermal fluids. The occurrence of these sinter, even if localized (e.g., sample O), could indicate upflow zones where geothermal fluids reach the surface. While the measured surface temperature of the TS is ~63° C, previous geothermometric studies in the area (Chiodini et al. 2014; JICA 1983; Tassi et al. 2016; Villalba 2023) indicate a deep reservoir temperature exceeding 150–200° C, classifying the Domuyo Geothermal System as high-enthalpy. The tectonic framework of the Andean Precordillera likely controls discharge locations, channeling these deep, high-temperature fluids through fault-controlled pathways (e.g., Rivas et al. 2024; Robidoux et al. 2025). This structural permeability is consistent with the regional deformation patterns described in the study area where fault intersections play a critical role in fluid migration (Galetto et al. 2018; Hurley et al. 2020; Villalba et al. 2025). In such systems, the precipitation of sinter occurs when these high-temperature, silica-saturated fluids experience rapid cooling and evaporation upon reaching the surface or near-surface environment, driving the polymerization of dissolved silica (Gunnarsson and Arnórsson 1999). The high H_4SiO_4 concentrations measured in TS confirm the potential for such precipitation under appropriate conditions.

The spatial distribution of the salts described in the study area, with travertines dominating in outflow zones and sinters indicating upflow areas, is a pattern observed in other geothermal systems of the Southern Andes (Benavente et al. 2016; Tardani et al. 2021; Wrage et al. 2017), and is consistent with the tectonic control exerted by the Andean Precordillera on fluid circulation (Rivas et al. 2024; Robidoux et al. 2025).

5.2 Hydrogeochemical Processes

The analysis of ionic composition and bivariate relationships reveals a clear spatial evolution of waters in the study area, from the headwaters to the zones influenced by the geothermal system. This evolution is governed by a complex interplay of magmatic, meteoric, and lithological controls, as evidenced by the distinct chemical signatures observed across different sampling sites and their spatial distribution.

5.2.1 Dissolution of Magmatic Gases and Carbonate Equilium

The relationship between Na^+ and Cl^- (Fig. 5a) reveals a clustering of TS along the 1:1 stoichiometric line, a signature characteristic of mature geothermal brines that have undergone extensive water-rock interaction and magmatic gas input (Giggenbach 1997; Vengosh et al. 2002). While the absolute concentrations of Na^+ and Cl^- in upstream waters (S-US, W-US) are significantly lower than in TS, their compositional facies (Ca-HCO_3) and ionic ratios (Ca^{2+} > Na^+, HCO_3^- > Cl^-) are consistent with those of meteoric waters interacting with surface rocks. In contrast, the 1:1 Na^+/Cl^- trend observed in TS is characteristic of geothermal fluids due to deep, high-temperature processes, as documented in other geothermal systems (Evans et al. 2004). The stoichiometry of these ions is often equivalent to that expected for typical geothermal brines, which can result from the enrichment of water by magmatic gases and high-temperature water-rock interaction. The dissolution of magmatic gases such as HCl and also SO_2 (which can later be oxidized to SO_4^{2-}) in hydrothermal groundwater contributes significantly to Cl^- and SO_4^{2-} concentrations (Llano et al. 2025; Tassi et al. 2016; Villalba et al. 2020). Additionally, high SO_4^{2-} contents in some areas could also be attributed to the oxidation of H_2S occurring at shallow depths, another process common in these geothermal environments (Tassi et al. 2016). The S-US and W-US display very low concentrations of the aforementioned ions. However, S-DS samples shows a significant compositional shift (e.g., ~2 orders of magnitude in Na^+ and Cl^- concentrations compared to S-US; Table 5), trending toward the chemical signatures observed in geothermal discharges (Fig. 5a). The enrichment in Na^+ concentration in TS (up to 81 mmol L^{-1}), as observed in the CO_3^{2-} + HCO_3^- ratios, differentiates it from the S-US and W-US (Na^+ up to 0.2 mmol L^{-1}). The S-DS and W-DS samples show a similar trend to TS, which is consistent with mixing processes between the aforementioned upstream waters and geothermal fluids, resulting in an intermediate composition (Fig. 5b). Theoretical calculations with conservative ions have been reported using upstream vs. downstream water compositions as extreme members, which yielded substantial percentages of mixing (10 to 47%; Villalba et al. 2022). Furthermore, $CO_{2(g)}$ has been identified as a major component of fumarolic emissions in this and other comparable geothermal systems, contributing to the HCO_3^- budget of these waters (Tassi et al. 2016).

On the other hand, despite likely interaction with Ca-bearing minerals at depth, TS exhibit low Ca^{2+} concentrations (except one sample reaching 4.5 mmol L^{-1}, Fig. 5c), which contrasts with their high anionic contents (SO_4^{2-}, HCO_3^-, Cl^-). This depletion is consistent with active

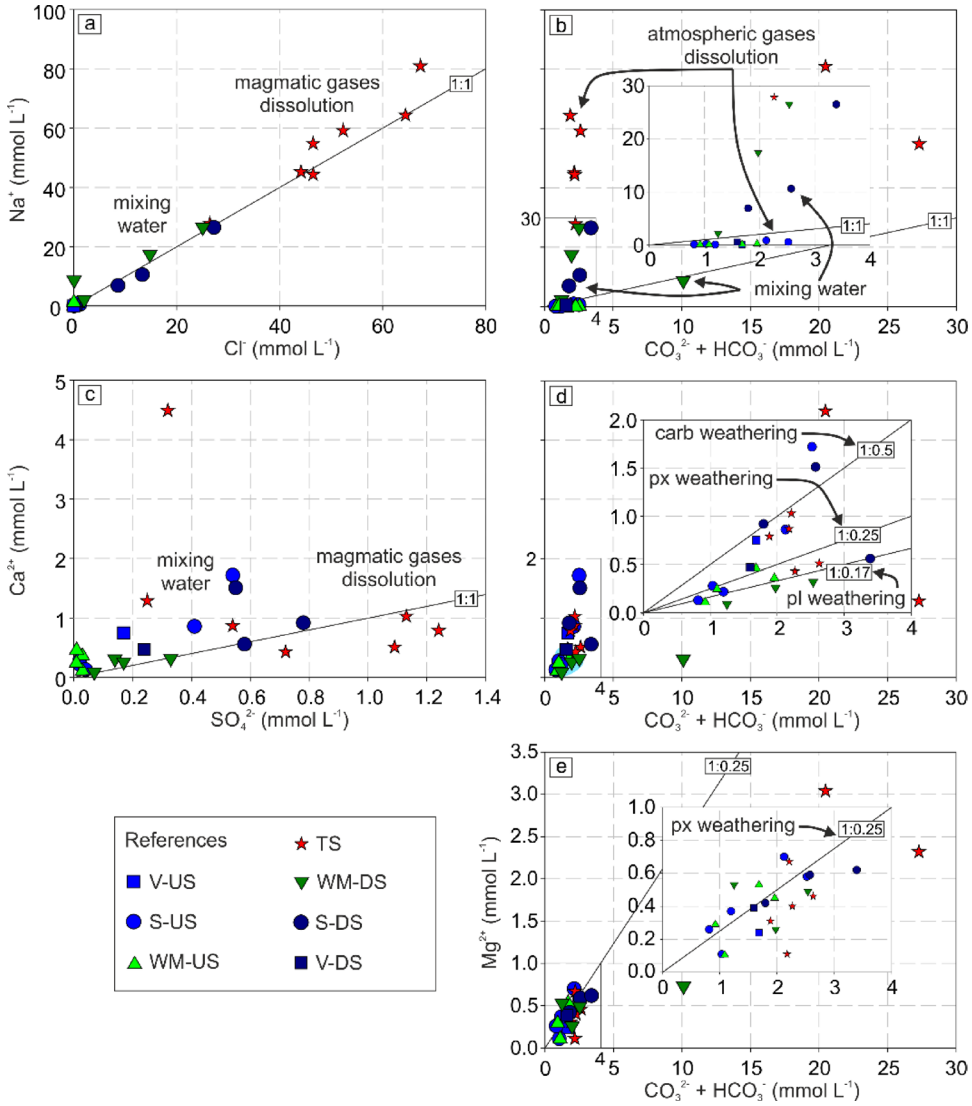

Fig. 5 Bivariate diagrams between the major cations and anions of cold and thermal water samples of the Domuyo Geothermal System with trend lines of mineral stoichiometric ratio and the main hydrogeochemical processes identified

carbonate precipitation as CO_2-rich waters degas (increasing pH) and cool upon surface discharge (Villalba et al. 2020; Villalba 2023), a process further discussed in Sect. 5.1. However, some TS samples plot above the 1:1 line, which likely reflects a transitional composition resulting from mixing with shallow groundwaters or extensive interaction with Ca-bearing host rocks (plagioclase and carbonates) at shallower depths, which enriches the fluid in Ca^{2+} relative to SO_4^{2-} (Fig. 5c). The observed travertine deposits provide direct evidence of this process, confirming that the waters are supersaturated with respect to calcite. In fact, previous geochemical modeling performed on these waters in the study area provides saturation index values for carbonate and silica minerals (Villalba et al. 2020). These values indicate that minerals such as calcite and aragonite are prone to precipitate (saturation index > 0), while silica group minerals tend to be in solution (generally saturation index < 0). As the fluid cools and loses CO_2, the equilibrium shifts toward precipitation, removing Ca^{2+} from solution. This phenomenon is also reflected in downstream samples (S-DS, W-DS), where Ca^{2+} concentrations remain relatively low compared to anions, indicating continued influence of carbonate precipitation even after mixing with cooler waters (Fig. 5c, d).

5.2.2 Chemical Weathering Associated with Water-Rock Interaction

The relationship between Ca^{2+} and $CO_3^{2-} + HCO_3^-$ indicates that most of the sampled waters are associated with the weathering of carbonates (~1:0.5), oligoclase-type plagioclase (~1:0.17), and pyroxenes (~1:0.25), mineral species present in the study area (Sect. 4.1.; Silva-Fragoso et al. 2021; Zanettini et al. 2001). For instance, in headwater areas such as El Humazo (stream number 3, Fig. 1), the dominant Ca^{2+}, HCO_3^-, and SO_4^{2-} contents are attributed to interaction with carbonate-matrix sedimentary rocks and

gypsum-bearing units reported in this sector (Zanettini et al. 2001). Conversely, high values of Ca^{2+} in the Manchana Covunco and Covunco streams, remaining relatively constant between headwater and lower basin (~1.6 mmol L^{-1} and ~0.9 mmol L^{-1}, respectively), are recorded without a clear correlation with anions, suggesting complex interactions or localized mineralogical controls (Fig. 5d).

The Varvarco river samples fit around the 1:1 line of the Ca^{2+} vs. SO_4^{2-} diagram, indicating the dissolution of gypsum or anhydrite from evaporites in the study area (Jurassic marine sedimentary rocks, Fig. 1). Notably, the V-DS sample shows a shift closer to this line, suggesting a minor contribution of geothermal-derived sulfate to the river chemistry (Fig. 5c). However, the overall composition of the river is strongly influenced by dilution. The discrepancy between the moderate geothermal impact observed in this study and the stronger signals reported in previous works (e.g., Chiodini et al. 2014; Llano et al. 2025; Tassi et al. 2016) is primarily attributed to seasonal hydrodynamic variations. The sampling was conducted in November for this work, coinciding with the austral spring snowmelt, when the river flow rate is at its peak (~69 m^3 s^{-1}). This high volume of meteoric water significantly dilutes the geothermal inputs (~0.5 m^3 s^{-1}), masking the chemical traces that are typically more evident during low-flow periods (late summer/autumn), as noted by Villalba et al. (2022). The seasonal dilution effect implies that the water quality of the Varvarco river for human and agricultural use is considerably higher during the snowmelt season compared to the baseflow period. This dilution mechanism was reported in several watersheds in the Andes (e.g., Macchioli-Grande et al. 2025; León and Pedrozo 2015), and is particularly relevant given the glacial and periglacial contributions to the hydrological budget described in the area (e.g., Falaschi et al. 2023). Despite this dilution, a slight input of Na^+ and Cl^- is detectable downstream, accompanied by elevated concentrations of typical geothermal trace elements (e.g., As, B) and increase in EC. This multiparametric signature confirms the influence of geothermal discharges (Fig. 5a). Such enrichments are consistent with previous hydrogeochemical characterizations of the area (Llano et al. 2025; Villalba et al. 2020, 2022), which identified these elements as reliable tracers of geothermal inputs even under high-flow conditions. Previously reported seasonal variations in the facies of the river (Ca-SO_4 or Ca-HCO_3 upstream to Na-SO_4/Cl or Ca/Mg-HCO_3 downstream) highlight the dynamic interplay between geothermal inputs and hydroclimatic conditions (Villalba et al. 2022).

Most of the samples show an increase in Mg^{2+} and CO_3^{2-} + HCO_3^- ions with a ratio close to 1:0.25 (Fig. 5e), consistent with pyroxene weathering (Zaidi et al. 2017), which is supported by the geological context of the study area, due to presence of mafic igneous rocks (e.g., LVC; Zanettini et al. 2001). Furthermore, the observed corrosion and coronitic textures in amphiboles (e.g., sample E) provide direct field evidence for the concurrent weathering of this additional Ca- and Mg-bearing mafic mineral. The ionic relationships established for the wet meadows also suggest the incorporation of Ca^{2+}, Mg^{2+} and HCO_3^- generated by the dissolution of silicates, such as anorthite and pyroxenes (Fig. 5d, e). Likewise, the Na^+ and HCO_3^- contents in the wet meadows and surface watercourses may originate from the albite dissolution (Fig. 5b).

Silica concentrations, measurable as the soluble species H_4SiO_4, also revealed marked differences among the various sampling groups (Table 5). S-US exhibited relatively low concentrations in this compound, while slightly higher values were observed in W-US. In contrast, TS displayed significantly elevated silica contents (up to 2.6 mmol L^{-1}), which likely reflects a prolonged water-rock interaction at high temperatures within the geothermal reservoir (~4 times greater compared with S-US and W-US). S-DS silica content indicates a partial inheritance of the TS signature. Similarly, W-DS showed high silica values consistent with the input of silica-rich waters and possibly extended residence time that favor further silicate dissolution. The H_4SiO_4 would be primarily associated with the hydrolysis of feldspars and silica group minerals such as tridymite, cristobalite, quartz, and non-crystalline silica in water, affecting not only deep-seated host rocks but also surface lithological materials (Arnórsson and Stefánsson 1999; Sadiq et al. 1980). In TS, high H_4SiO_4 contents are related to the water-rock interaction during underground thermal circulation and the subsequent hydrolysis of feldspars and silica minerals present in the underlying rocks, aided by high temperatures (Gunnarsson and Arnórsson 1999).

In headwater areas, the slightly higher H_4SiO_4 values in W-US compared to S-US suggest localized weathering of surface volcanic materials or poorly developed soils rich in non-crystalline silica. Given the geology of the study area (dominated by volcanic rocks of the Lower and Upper Volcanic cycles), the contribution of silica to the water is expected to originate from the weathering of volcanic glass, which is characterized by its high solubility (Stumm and Morgan 1996). This differentiation in the crystallinity of the minerals involved also explains the high concentration of H_4SiO_4 despite not being associated with high temperature like TS, since non-crystalline silica is thermodynamically more soluble than quartz (e.g., Gunnarsson and Arnórsson 1999). High H_4SiO_4 concentrations in samples from downstream reflect both thermal input and the dissolution of non-crystalline silica at the surface. The latter processes would also be due to subsurface (wet meadows) and surface (streams and river) circulation of water through the rocky

substrate covering the study area or through poorly developed soils containing these minerals (Sadiq et al. 1980).

5.2.3 Base Exchange Processes and Cation Mobility

The ratio between $Na^+ + K^+$ and $H_4SiO_4 + HCO_3^-$ shows that most surface watercourses in headwaters and W-US have low relative cation contents and variable quantities of H_4SiO_4 and HCO_3^- (Fig. 6a). In this distribution, these samples are positioned close to the $H_4SiO_4 + HCO_3^-$ axis, which would reflect that the predominant process is associated with silicate weathering over base exchange processes (Emvoutou et al. 2018). Most of TS record a clear shift toward higher $Na^+ + K^+$, suggesting the prevalence of base exchange processes, although two samples fall within the field of silicate weathering processes (Emvoutou et al. 2018) (Fig. 6b). This base exchange can be mechanistically understood as the release of Na^+ from adsorption surfaces on clay minerals (e.g., illite, smectite) and zeolites formed during hydrothermal alteration (Sect. 5.1), into the geothermal fluids, in exchange for divalent cations such as Ca^{2+} (Mas et al. 2000; Villalba et al. 2020, 2022). According to the Hofmeister series, divalent cations (Ca^{2+}, Mg^{2+}) are preferentially adsorbed onto clay surfaces compared to monovalent cations (Na^+, K^+) (e.g., Stumm and Morgan 1996). Therefore, the Ca^{2+}-rich geothermal fluids can displace Na^+ from these surfaces, releasing Na^+ into the solution. This interpretation is further supported by microanalytical data from secondary minerals in the study area. EDAX analysis of zeolites (mordenite and heulandite) shows a significantly higher abundance of Ca^{2+} compared to Na^+ (see Fig. 6a, c in Mas et al. 2000). In contrast, tridymite, a silica mineral, exhibits more balanced Ca^{2+} and Na^+ contents. This compositional difference would reflect the preferential adsorption of Ca^{2+}over Na^+ on the surfaces of zeolitic minerals, consistent with the Hofmeister series (e.g., Depetris et al. 2014).

Interestingly, two TS samples (TS-1 and TS-2; Table 5) fall within the field of silicate weathering, diverging from the main geothermal trend. These samples likely represent peripherical discharges where the primary geothermal signature is masked by significant mixing with shallow groundwaters. Unlike the mature geothermal fluids dominated by

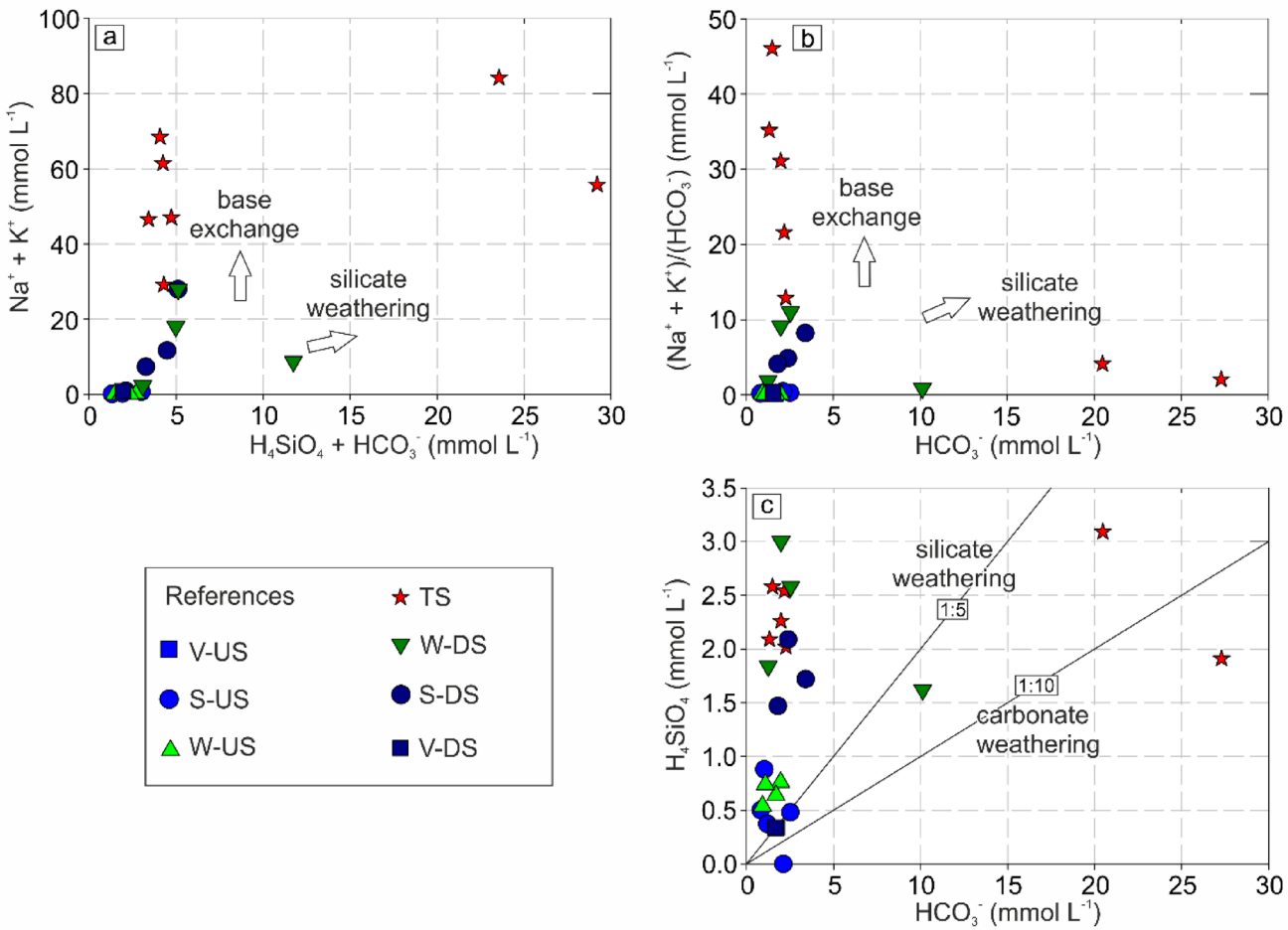

Fig. 6 Ionic ratios in the studied water samples where monovalent cations are related to silica and bicarbonate (**a**), monovalent cations and bicarbonate (**b**), and bicarbonate with silicic acid (**c**)

base exchange, the chemistry of these specific springs is controlled by the silicate weathering typical of the shallow meteoric aquifers, a hypothesis supported by their relatively lower T and peripheral location (Fig. 1c), possibly reflecting variable residence times or heterogeneous mineralogy within the geothermal system (Fig. 6a). Downstream samples (S-DS, W-DS) exhibit intermediate behaviour, consistent with mixing and progressive ion exchange along flow paths (Fig. 6a, b). The same trends were recorded for each sample group based on relationships among Na^+, K^+ and HCO_3^-, where processes associated with silicate weathering are observed in upstream sectors, and then the behaviour deviates towards base exchange for TS and S-DS samples (Fig. 6b).

Finally, to further discriminate between carbonate and silicate weathering based on H4SiO4 and HCO3− concentrations were compared (Zaidi et al. 2017). This analysis places the majority of samples within the silicate weathering field, with a ratio lower than 1:5 (Fig. 6c). However, in the high-enthalpy context of the Domuyo Geothermal System, particularly for TS samples, this hydrogeochemical signature is not solely a function of primary mineral dissolution but is significantly modulated by reservoir thermodynamics and gas-water interactions. While the input of magmatic CO2 provides a continuous source of bicarbonate, the ratio is also governed by the temperature-dependent solubility of silica. The high reservoir temperatures enhance the hydrolysis of the silicates, resulting in elevated H4SiO4 concentrations that effectively override the fluctuations in HCO3− levels caused by CO2 uptake or secondary calcite precipitation. Consequently, the observed dominance of the silicate weathering trend in TS confirms that, despite the active carbonate system, the water chemistry is ultimately controlled by the thermal equilibration with the host rocks. Exceptions include one TS sample and one S-US sample with ratios greater than 1:10, which is suggestive of localized carbonate weathering; and two samples (one W-DS and one TS) showing intermediate ratios, likely reflecting mixed sources or transitional zones.

5.3 Hydrogeochemical Conceptual Model

A conceptual model that integrates the dominant hydrogeochemical processes and ionic contributions identified for each sector of the studied water system is presented, including both secondary transformations and precipitation processes that influence water chemistry.

In the S-US samples, ionic inputs primarily derive from the dissolution of plagioclase (contributing Na^+, Ca^{2+}), sedimentary rocks (releasing Ca^{2+} and Mg^{2+}, and potentially in carbonate-rich units, HCO_3^- and CO_3^{2-}), and the dissolution of atmospheric gases (CO_2, generating HCO_3^- and CO_3^{2-}) which facilitates weathering. Contribution derived from base exchange processes is also identified, where Na^+ from the rocks can be released into the water in exchange for other cations. These processes, along with general silicate weathering including volcanic glass (an important source of initial H_4SiO_4) result in waters with a mixed signature, and define their baseline composition (Fig. 7a).

W-US samples exhibit a hydrogeochemical functioning similar to that of streams in this sector. The dissolution of plagioclase is a key source of ions (notably HCO_3^-, CO_3^{2-}, and variable Na^+, Ca^{2+}, and Mg^{2+} inputs). However, water-rock interaction in these wet meadows appears limited, likely due to physicochemical conditions that are unfavorable for extensive mineral dissolution and the typically short residence times of waters within these environments (Fig. 7b).

TS samples are the surface manifestation of a complex deep geothermal system. Their chemistry represents a drastically different hydrogeochemical system, fed by the input of deep geothermal waters (e.g., Tassi et al. 2016). These waters ascend, and their composition is marked by the dissolution of various types of feldspars and other silicate minerals at high temperatures, which significantly increases the concentration of dissolved ions (e.g., EC up to 8450 µS cm^{-1}). A crucial component is the input of magmatic gases (such as HCl, SO_2 and CO_2), which upon dissolving in the deep geothermal water (Cl^-, SO_4^{2-}, HCO_3^-, and CO_3^{2-}) define the anionic facies and initial acidity that can enhance rock dissolution. Base exchange also plays a role, modifying cationic ratios (Na^+ contribution). This solute- and H_4SiO_4 -enriched water, upon ascending and discharging at the surface, undergoes significant changes: (i) CO_2 degassing and cooling cause the precipitation of calcite, forming the observed travertine deposits and explaining the sometimes low Ca^{2+} concentrations in the discharged thermal water, and (ii) cooling of these silica-saturated waters can lead to the precipitation of non-crystalline silica, contributing to the formation of siliceous sinters, if conditions are favorable. These precipitation processes are a direct manifestation of water-rock interaction and physicochemical changes in the discharge zone (Fig. 7c).

W-DS samples reflects a clear influence by geothermal water input (mainly Na^+ and Cl^- contribution). However, their final composition is also modulated by local processes such as base exchange, influenced by the new ionic composition of the water, and the continuous dissolution of reactive surface materials like volcanic glass or non-crystalline silica, which contribute H_4SiO_4. The influence of meltwater in these wet meadows may also favor soil and substrate leaching processes (Fig. 7d).

S-DS samples are significantly impacted by the geothermal water input (Na^+ and Cl^- contribution). This influence

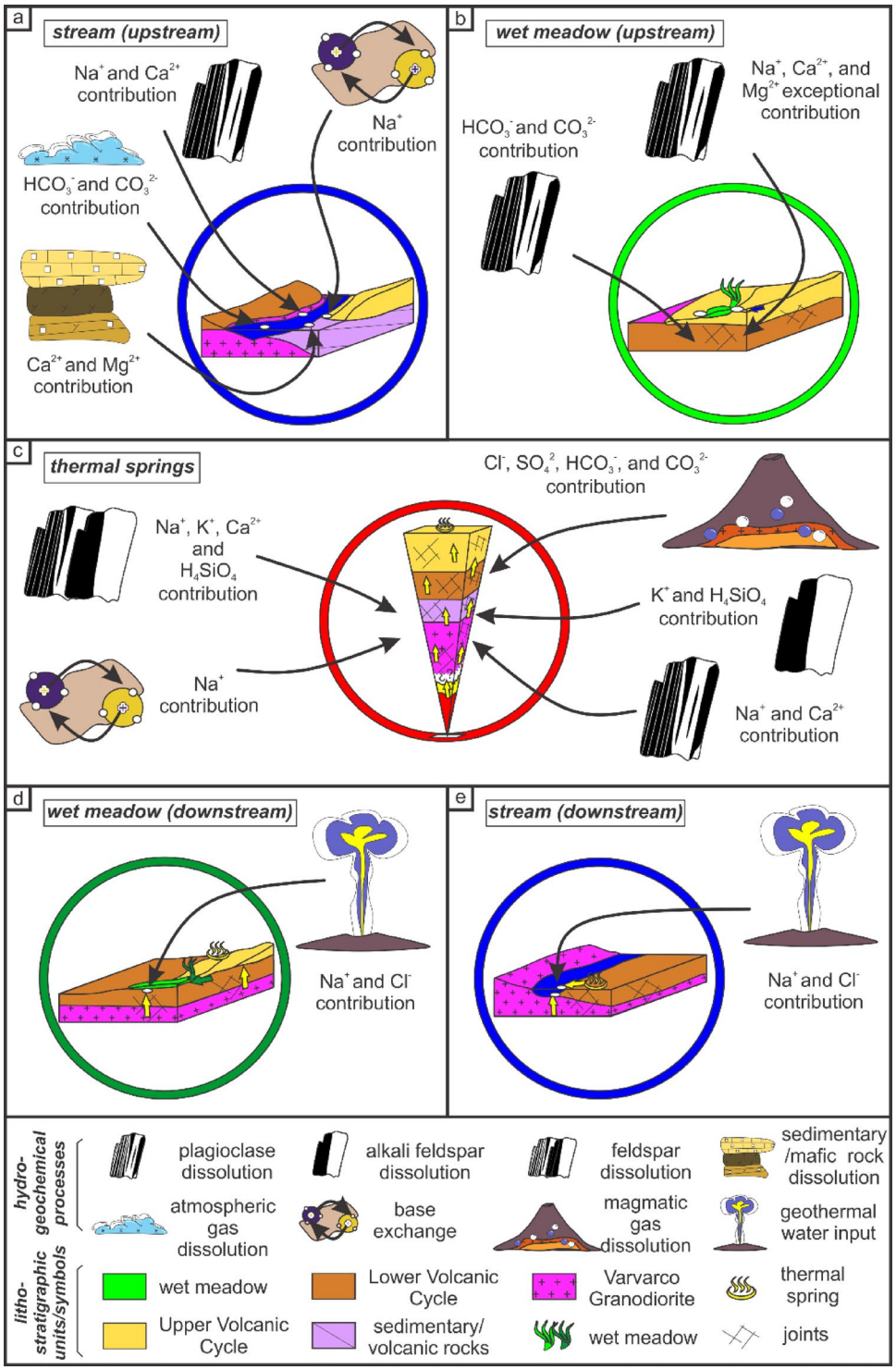

Fig. 7 Hydrogeochemical conceptual modelling on functioning of each sector in the system studied. Block diagrams of the surface watercourses and wet meadows in headwater sector (**a**, **b**), of the thermal springs (**c**), and the surface watercourses in lower basin sector (**d**, **e**) are shown

of thermal waters modifies the composition that the watercourses carry from the headwaters, superimposing a saline (Na-Cl) signature onto the original silicate and/or carbonate weathering signal. In addition to this mixing, processes such as base exchange and the volcanic glass dissolution or non-crystalline silica in the stream bed and banks can continue to modify the water composition and H_4SiO_4 levels downstream from the main discharge area (Fig. 7e).

6 Conclusions

This study investigated the hydrogeochemical processes governing water composition in the Domuyo Geothermal System, integrating the geochemistry of surface waters, the mineralogy of host rocks, and the characteristics of hydrothermal precipitates. The findings reveal a complex interplay between deep geothermal processes and shallow meteoric circulation, all modulated by the tectonic framework of the region.

The waters of the upstream sectors are Ca-HCO_3, reflecting low-temperature water-rock interaction with local volcanic and sedimentary rocks. In contrast, the thermal springs exhibit Na-Cl composition, with high concentrations of HCO_3^- and H_4SiO_4, indicative of a high-temperature water-rock interaction and the input of magmatic volatiles as dominant processes. The chemical composition of waters in the downstream sector represents a mixture of these two end-members. This mixing, combined with secondary processes such as carbonate precipitation (evidenced by widespread travertine formation) and cation exchange with secondary clay minerals formed during hydrothermal alteration, shaped the final hydrogeochemical signature of the system. The integration of rock, water, and precipitate data not only provides a robust framework for understanding the evolution of the system, but also establishes a critical hydrogeochemical baseline. Finally, this integrated model demonstrates its utility for the sustainable management of water resources in vulnerable geothermal-meteoric interface zones, serving as a key tool to anticipate quality changes in downstream supplies.

Acknowledgements The authors would like to thank the Neuquén government authorities for granting them permission to conduct research in the Domuyo Natural Protected Area (ANPD), the Faculty of Natural Sciences and Museum (FCNyM, UNLP), and the CONICET for their financial support (Award N114/22 to EV from FCNyM) and technical facilities.

Funding This research was funded by a CONICET Postdoctoral fellowship awarded to EV, and a grant N114/22 from FCNyM-UNLP to EV.

Declarations

Competing interests The authors declare that they have no known competing financial interests or personal relationships that could have appeared to influence the work reported in this paper.

References

Alao JO (2023) Impacts of open dumpsite leachates on soil and groundwater quality. Groundw Sustain Develop 20:100877. https://doi.org/10.1016/j.gsd.2022.100877

Alao JO (2025a) Understanding the interactions between uncaptured landfill plume Contaminants, Soil, groundwater Resources, public health Systems, and their implications. Environm Pollut 127190. https://doi.org/10.1016/j.envpol.2025.127190

Alao JO, Abubakar F (2025) Groundwater exploration, management strategies and sustainability: geophysical approaches. GeoGeo 4(3):100395. https://doi.org/10.1016/j.geogeo.2025.100395

Alao JO, Bello AY, Lawal HA, Abdullahi D (2024a) Assessment of groundwater challenge and the sustainable management strategies. Result Earth Sci 2:100049. https://doi.org/10.1016/j.rines.2024.100049

Alao JO, Eze SU, Onyenweife GI, Ibe AA, Otorkpa OJ, Ayejoto DA, Abubakar F, Abdulsalami M, Abdulmalik DO (2025b) Enhancing water security through integrated storage mechanisms and rainwater harvesting for sustainable development. Discov Sustain 6:941. https://doi.org/10.1007/s43621-025-01914-2

Alao JO, Lawal HA, Abdulsalami M, Abubakar F, Abduwahab OO, Mary ET, Yusuf MA (2024b) Delineation of aquifer storage potential in response to regional groundwater development. Discov Water 4:25. https://doi.org/10.1007/s43832-024-00084-y

Alao JO, Yusuf MA, Nur MS, Nuruddeen AM, Ahmad MS, Jaiyeoba E (2023) Delineation of aquifer promising zones and protective capacity for regional groundwater development and sustainability. SN Appl Sci 5(5):149. https://doi.org/10.1007/s42452-023-05371-2

APHA (1998) Standard methods for the examination of water and wastewater, 20th edn. American Water Works Association, Water Environment Federation

Arnórsson S, Stefánsson A (1999) Assessment of feldspar solubility constants in water in the range of 0 degrees to 350 degrees C at vapor saturation pressures. Am J Sci 299(3):173–209. https://doi.org/10.2475/ajs.299.3.173

Arnórsson S, Stefánsson A, Bjarnason JO (2007) Fluid-fluid interactions in geothermal systems. Rev Mineral Geochem 65(1):259–312. https://doi.org/10.2138/rmg.2007.65.9

Benavente O, Tassi F, Reich M, Aguilera F, Capecchiacci F, Gutiérrez F, Vaselli O, Rizzo A (2016) Chemical and isotopic features of cold and thermal fluids discharged in the Southern volcanic zone between 32.5°S and 36°S: insights into the physical and chemical processes controlling fluid geochemistry in geothermal systems of central Chile. Chem Geol 420:97–113. https://doi.org/10.1016/j.chemgeo.2015.11.010

Benmarce K, Hadji R, Hamed Y, Zahri F, Zighmi K, Hamad A, Gentilucci M, Ncibi K, Besser H (2023) Hydrogeological and water quality analysis of thermal springs in the Guelma region of North-Eastern algeria: A study using hydrochemical, statistical, and isotopic approaches. J Afr Earth Sci 205:105011. https://doi.org/10.1016/j.jafrearsci.2023.105011

Brousse R, Pesce AH (1982) Cerro domo: Un volcán cuartario Con posibilidades geotérmicas, provincia Del Neuquén, Argentina. V Congreso Latinoamericano de Geología, Buenos Aires, Argentina

Capezzuoli E, Gandin A, Pedley M (2014) Decoding Tufa and travertine (fresh water carbonates) in the sedimentary record: the state of the Art. Sedimentology 61(1):1–21

Chalise B, Paudyal P, Kunwar BB, Bishwakarma K, Thapa B, Pant RR, Neupane BB (2023) Water quality and hydrochemical assessments of thermal springs. Gandaki Province Nepal Heliyon 9(6):e17353. https://doi.org/10.1016/j.heliyon.2023.e17353

Chiodini G, Liccioli C, Vaselli O, Calabrese S, Tassi F, Caliro S, Caselli A, Agusto M, D'Alessandro W (2014) The Domuyo volcanic system: an enormous geothermal resource in Argentina patagonia. J Volcanol Geoth Res 274:71–77. https://doi.org/10.1016/j.jvolgeores

Daniele L, Taucare M, Viguier B, Arancibia G, Aravena D, Roquer T, Sepúlveda J, Molina E, Delgado A, Muñoz M, Morata D (2020) Exploring the shallow geothermal resources in the Chilean Southern volcanic zone: insight from the Liquiñe thermal springs. J Geochem Explor 218:106611. https://doi.org/10.1016/j.gexplo.2020.106611

D'Elia L, Páez G, Hernando IR, Petrinovic IA, López L, Kürten G, Vigiani L (2020) Hydrothermal eruptions at El Humazo, Domuyo geothermal field, argentina: insights into the eruptive dynamics and controls. J Volcanol Geoth Res 393:106786. https://doi.org/10.1016/j.jvolgeores.2020.106786

Dellapé DA, Pando GA, Uliana MA, Musacchio EA (1978) Foraminíferos y ostrácodos Del Jurásico En Las inmediaciones Del Arroyo Picún Leufú y La Ruta 40 (provincia Del Neuquén, Argentina), Con Algunas Consideraciones sobre La estratigrafía de La Formación Lotena. VII Congreso Geológico Argentino, Neuquén, Argentina

Depetris PJ, Pasquini AI, Lecomte KL (2014) Weathering and the riverine denudation of continents. Springer Briefs in Earth System Sciences. https://link.springer.com/book/https://doi.org/10.1007/978-94-007-7717-0

Dobson PF, Salah S, Spycher N, Sonnenthal EL (2004) Simulation of water–rock interaction in the Yellowstone geothermal system using TOUGHREACT. Geothermics 33(4):493–502. https://doi.org/10.1016/j.geothermics.2003.10.002

Eichelberger J (2020) Distribution and transport of thermal energy within magma–hydrothermal systems. Geosciences 10(6):212. https://doi.org/10.3390/geosciences10060212

Emvoutou HC, Ketchemen Tandia B, Ngo Boum Nkot S, Ebonji RCS, Nlend YB, Ekodeck GE, Stumpp C, Maloszewski P, Faye S (2018) Geologic factors controlling groundwater chemistry in the coastal aquifer system of Douala/Cameroon: implication for groundwater system functioning. Environ Earth Sci 77:1–23. https://doi.org/10.1007/s12665-018-7400-z

EOS Trans Am Geophys Union 25(6):914–928. https://doi.org/10.1029/TR025i006p00914

Evans MJ, Derry LA, France-Lanord C (2004) Geothermal fluxes of alkalinity in the Narayani river system of central Nepal. Geochem Geophys Geosyst. https://doi.org/10.1029/2004GC000719

Falaschi D, Berthier E, Belart JMC, Bravo C, Castro M, Durand M, Villalba R (2023) Increased mass loss of glaciers in Volcán Domuyo (Argentinian Andes) between 1962 and 2020, revealed by aerial photos and satellite stereo imagery. J Glaciol 69(273):40–56. https://doi.org/10.1017/jog.2022.4

Fouke BW, Farmer JD, Des Marais DJ, Pratt L, Sturchio NC, Burns PC, Discipulo MK (2000) Depositional facies and aqueous-solid geochemistry of travertine-depositing hot springs (Angel Terrace, mammoth hot Springs, Yellowstone National Park, U.S.A). J Sediment Res 70(3):565–585. https://doi.org/10.1306/2dc40929-0e47-11d7-8643000102c1865d

Fournier RO (1999) Hydrothermal processes related to movement of fluid from plastic into brittle rock in the magmatic-epithermal environment. Econ Geol 94(8):1193–1211. https://doi.org/10.2113/gsecongeo.94.8.1193

Galetto A, García V, Caselli A (2018) Structural controls of the Domuyo geothermal field, Southern Andes (36 38′ S), Argentina. J Struct Geol 114:76–94. https://doi.org/10.1016/j.jsg.2018.06.002

Giggenbach WF (1996) Chemical composition of volcanic gases. In: Scarpa R, Tilling RI (eds) Monitoring and mitigation of volcano hazards Springer Berlin Heidelberg, Berlin, Heidelberg, pp 221–256

Giggenbach WF (1997) The origin and evolution of fluids in magmatic-hydrothermal systems. In: Barnes HL (ed) Geochemistry of hydrothermal ore deposits, 3rd edn. Wiley, New York, pp 737–796

Gulisano CA, Gutiérrez Preimling AR, Digregorio RE (1984) Esquema estratigráfico de La secuencia jurásica Del Oeste de La provincia Del Neuquén. IX Congreso Geológico Argentino, San Carlos de Bariloche, Argentina

Gunnarsson I, Arnórsson S (1999) New data on the standard Gibbs energy of H_4SiO_4 and its effect on silicate solubility. In: Ármannsson H (ed) Geochemistry of the earth's surface. Balkema, Rotterdam, pp 449–452

Hem JD, Cropper WH (1960) Chemistry of Iron in Natural Water. Geol Surv Water Supply 1459

Hervé M, Suárez M, Puig A (1984) The Patagonian batholith S of Tierra Del Fuego, chile: timing and tectonic implications. J Geol Soc 141(5):909–917. https://doi.org/10.1144/gsjgs.141.5.0909

Holdren JGR, Berner RA (1979) Mechanism of feldspar weathering-I. Experimental studies. Geochim Cosmochim Acta 43(8):1161–1171. https://doi.org/10.1016/0016-7037(79)90109-1

Hurley M, Colavitto B, Astort A, Sagripanti L, Rosselot EA, Folguera A (2020) Mass-wasting deposits in the Domuyo volcanic Center, Northern Neuquén andes (Argentina): an analysis of the controlling factors. J South Am Earth Sci 103:102760. https://doi.org/10.1016/j.jsames.2020.102760

Ingebritsen SE, Manning CE (1999) Geological implications of a permeability-depth curve for the continental crust. Geol 27(12):1107–1110. https://doi.org/10.1130/0091-7613(1999)027%3C1107:gioapd%3E2.3.co

JICA (1983) Argentine Republic. Interim report on the Northern Neuquén geothermal development Project. First-second phase survey. Unpublished

Kele S, Breitenbach SF, Capezzuoli E, Meckler AN, Ziegler M, Millan IM, Kluge T, Deák J, Hanselmann K, John CM, Yan H, Liu Z, Bernasconi SM (2015) Temperature dependence of oxygen-and clumped isotope fractionation in carbonates: a study of travertines and tufas in the 6–95ºC temperature range. Geochim Cosmochim Acta 168:172–192. https://doi.org/10.1016/j.gca.2015.06.032

Kietzmann DA, Vennari VV (2013) Sedimentología y estratigrafía de La Formación Vaca muerta (Tithoniano-Berriasiano) En El área Del Cerro Domuyo, Norte de Neuquén. Argentina Geol 40(1):41–65. https://doi.org/10.5027/andgeo

Leanza HA (1972) Acantholissonia, Nuevo género de ammonites Del Valanginiano de Neuquén, Argentina, y Su posición estratigráfica. Rev Asoc Geol Argent 17(4):63–70

Leanza HA, Hugo CA (1997) Hoja Geológica 3969-III, Picún Leufú, provincias Del Neuquén y Río Negro. Servicio Geológico Minero Argentino, Buenos Aires

Lee KC (2001) Classification of geothermal resources by exergy. Geothermics 30(4):431–442. https://doi.org/10.1016/S0375-6505(00)00056-0

León JG, Pedrozo FL (2015) Lithological and hydrological controls on water composition: evaporite dissolution and glacial weathering in the South central Andes of Argentina (33–34 S). Hydrol Process 29(6):1156–1172. https://doi.org/10.1002/hyp.10226

Llambías EJ, Danderfer J, Palacios M, Brogioni N (1978) Las Rocas ígneas cenozoicas Del Volcán Domuyo y aéreas adyacentes. VII Congreso Geológico Argentino, Neuquén, Argentina

Llambías EJ, Leanza HA (2005) Depósitos Laháricos En La Formación Los Molles En Chacay Melehue, Neuquén: evidencia de Volcanismo jurásico En La Cuenca neuquina. Rev Asoc Geol Argent 60(3):552–558. www.scielo.org.ar/pdf/raga/v60n3/v60n3a10.pdf

Llambías EJ, Stipanicic PN (2002) Grupo Choiyoi. In: Stipanicic PN, Marsicano C (eds) Léxico Estratigráfico de la Argentina, Triásico, Asociación Geológica Argentina, Buenos Aires 89–91

Llano J, Li Vigni L, Agusto M, Brusca L, Caselli A, Chiodini G, D'Alessandro W, Lelli M, Tassi F, Vaselli O, Calabrese S (2025) Hydrogeochemical processes governing the origin, mobility and transport of trace elements in the Domuyo volcanic complex geothermal system (Patagonia, Argentina). J Volcanol Geoth Res 462:108322. https://doi.org/10.1016/j.jvolgeores.2025.108322

López-Escobar L, Cembrano J, Moreno H (1995) Geochemistry and tectonics of the Chilean Southern Andes basaltic quaternary volcanism (37–46 S). Geol 22(2):219–234

Macchioli-Grande M, Soto-Maass A, Pfeiffer M, Covarrubias JI, Peña-Echeverría A, Perez-Fodich A (2025) Solute generation and transport in semiarid mountain catchments of the central Chilean Andes. Earth Syst Environ 1–20. https://doi.org/10.1007/s41748-025-00642-x

Marshall RR (1961) Devitrification of natural glass. Geol Soc Am Bull 72(10):1493–1520. https://doi.org/10.1130/0016-7606(1961)72[1493:DONG]2.0.CO;2

Mas GR, Bengochea L, Mas LC (2000) Hydrothermal alteration at El Humazo geothermal area, Domuyo volcano, Argentina. Proceedings of the World Geothermal Congress, Tohoku, Japan. https://www.geothermal-energy.org/pdf/IGAstandard/WGC/2000/R0211.PDF

Mazzoni MM (1986) Procesos y Depósitos Piroclásticos. Asociación Geológica Argentina, Buenos Aires, Argentina. Serie B(14)

Narciso V, Santamaría G, Zanettini JCM (2004) Hoja Geológica 3769-1, Barrancas. Provincias de Mendoza y Neuquén. Instituto de Geología y Recursos Minerales, Servicio Geológico Minero Argentino. https://repositorio.segemar.gov.ar/handle/308849217/98

Palacios PR, Bustamante A, Romero-Gómez P, González JC (2011) Kinetic study of the thermal transformation of limonite to hematite by X-ray diffraction, -Raman and Mössbauer spectroscopy. Hyperfine Interact 203(1):113–118. https://doi.org/10.1007/s10751-011-0352-2

Panarello H, Sierra JL, D'amore F, Pedro G (1992) Isotopic and geochemical study of the Domuyo geothermal field, Neuquén Argentina. In: Proceeding of a meeting on nuclear techniques in geothermal resources investigation. San José, Costa Rica: International Atomic Energy Agency, Technical Document 641:31–56

Pentecost A (2005) Travertine. Springer Netherlands, Dordrecht

Pentecost A, Viles H (1994) A review and reassessment of travertine classification. Géographie Phys Et Quaternaire 48(3):305–314. https://doi.org/10.7202/033011ar

Pesce AH (1981) Estratigrafía de Las nacientes Del río Neuquén y Nahuever, provincia Del Neuquén. VIII Congreso Geológico Argentino, San Luis, Argentina

Piper AM (1944) A graphic procedure in the geochemical interpretation of water-analyses. https://doi.org/10.1029/TR025i006p00914

Ramos VA (1978) Estructura. In: Rolleri EO (ed.) Geología y recursos naturales de la Provincia del Neuquén, VII Congreso Geológico Argentino, Neuquén 99–118

Ramos VA (1999) Plate tectonic setting of the Andean cordillera. Episodes 22(3):183–190. https://doi.org/10.18814/epiiugs/1999/v22i3/005

Rapela CW, Llambías EJ (1985) Evolución magmática y relaciones regionales de Los complejos eruptivos de La Esperanza, provincia de Río Negro. Rev Asoc Geol Argent 40(1–2):4–25

Reinoso Carbonell VV, Campodonico VA, Alasino PH (2025) Origin of thermal waters in the Fiambalá basin (Argentina): preliminary insights from hydrochemistry and isotopic tracers. Geothermics 132:103434. https://doi.org/10.1016/j.geothermics.2025.103434

Reyes AG, Trompetter WJ (2012) Hydrothermal water–rock interaction and the redistribution of Li, B and Cl in the Taupo volcanic Zone, new Zealand. Chem Geol 314–317:96–112. https://doi.org/10.1016/j.chemgeo.2012.05.002

Rivas S, Sanchez-Alfaro P, Alvarez-Amado F, Perez-Fodich A, Godfrey L, Becerra P, Tardani D, Perez-Flores P, Aron F, Fica C, Munoz-Saez C, Mathur R (2024) Water-rock interaction and magmatic contribution in thermal fluids of the Southern volcanic Zone, chile: insights from Li, B and Sr isotopes. J Volcanol Geoth Res 453:108149. https://doi.org/10.1016/j.jvolgeores.2024.108149

Robidoux P, Tardani D, Sánchez-Alfaro P, Liuzzo M, Morata D, Moussallam Y, Rose-Koga E, Tassi F, Pérez-Flores P, Grassa F, Francofonte V (2025) Relationship of magmatic fluids to high-enthalpy geothermal systems: new insights from the Tolhuaca geothermal system (TGS), Southern Andes. Chem Geol 681:122583. https://doi.org/10.1016/j.chemgeo.2024.122583

Rodell M, Famiglietti JS, Wiese DN, Reager JT, Beaudoing HK, Landerer FW, Lo MH (2018) Emerging trends in global freshwater availability. Nature 557(7707):651–659. https://doi.org/10.1038/s41586018-0123-1

Rodgers KA, Browne PRL, Buddle TF, Cook KL, Greatrex RA, Hampton WA, Herdianita NR, Holland GR, Lynne BY, Martin R, Newton Z, Pastars D, Sannazarro KL, Teece CIA (2004) Silica phases in sinters and residues from geothermal fields of new Zealand. Earth Sci Rev 66:1–61. https://doi.org/10.1016/j.earscirev.2003.10.001

Sadiq M, Bledsoe BE, Enfield CG (1980) Solubility relationships of silica in soils. Comm Soil Sci Plant Anal 11(3):317–326. https://doi.org/10.1080/00103628009367038

Scanlon BR, Fakhreddine S, Rateb A, de Graaf I, Famiglietti J, Gleeson T, Grafton RQ, Jobbagy E, Kebede S, Kolusu SR, Konikow LF, Long D, Mekonnen M, Schmied HM, Mukherjee A, MacDonald A, Reedy RC, Shamsudduha M, Simmons CT, Sun A, Taylor RG, Villholth KG, Vörösmarty CJ, Zheng C (2023) Global water resources and the role of groundwater in a resilient water future. Nat Rev Earth Environ 4(2):87–101. https://doi.org/10.1038/s43017-022-00378-6

Silva-Fragoso A, Ferrari L, Norini G, Orozco-Esquivel T, Corbo-Camargo F, Bernal JP, Castro C, Arrubarrena-Moreno M (2021) Geology and conceptual model of the Domuyo geothermal area, Northern Patagonia, Argentina. J Volcanol Geoth Res 420:107396. https://doi.org/10.1016/j.jvolgeores.2021.107396

Spalletti LA, Arrondo OG, Morel E, Ganuza DG (1991) Evidencias sobre La edad triásica de La Formación Lapa En La región de Chacaico (Provincia Del Neuquén). Rev Asoc Geol Argent 46(3–4):167–172

Stefánsson A, Arnórsson S, Sveinbjörnsdóttir ÁE, Heinemaier J, Kristmannsdóttir H (2019) Isotope (δD, $\delta^{18}O$, ^{3}H, $\delta^{13}C$, ^{14}C) and chemical (B, Cl) constrains on water origin, mixing, water-rock interaction and age of low-temperature geothermal water. Appl Geochem 108:104380. https://doi.org/10.1016/j.apgeochem.2019.104380

Stern CR (2004) Active Andean volcanism: its geologic and tectonic setting. Revista Geol Chile 31(2):161–206. https://doi.org/10.4067/S0716-02082004000200001

Stipanicic PN, Rodrigo F, Baulíes OL, Martínez CG (1968) Las formaciones presenonianas En El denominado Macizo Nordpatagónico y regiones adyacentes. Rev Asoc Geol Argent 23(2):367–388

Streckeisen A (1980) Classification and nomenclature of volcanic rocks, lamprophyres, carbonatites and melilitic rocks IUGS subcommission on the systematics of igneous rocks: recommendations and suggestions. Geol Rundsch 69(1):194–207. https://doi.org/10.1007/BF01869032

Stumm W, Morgan JJ (1996) Aquatic chemistry. Chemical equilibria and rates in natural waters, 3rd edn. Wiley

Tardani D, Roulleau E, Pinti DL, Pérez-Flores P, Daniele L, Reich M, Sanchez-Alfaro P, Morata D, Richard L (2021) Structural control on shallow hydrogeochemical processes at Caviahue-Copahue volcanic complex (CCVC), Argentina. J Volcanol Geoth Res 414:107228. https://doi.org/10.1016/j.jvolgeores.2021.107228

Tassi F, Liccioli C, Agusto M, Chiodini G, Vaselli O, Calabrese S, Pecoraino G, Tempesti L, Caponi C, Fiebig J, Caliro S, Caselli A (2016) The hydrothermal system of the Domuyo volcanic complex (Argentina): A conceptual model based on new geochemical and isotopic evidences. J Volcanol Geoth Res 328:198–209. https://doi.org/10.1016/j.jvolgeores.2016.11.003

Taucare M, Viguier B, Figueroa R, Daniele L (2024) The alarming state of central chile's groundwater resources: A paradigmatic case of a lasting overexploitation. Sci Total Environ 906:167723. https://doi.org/10.1016/j.scitotenv.2023.167723

Teruggi ME, Mazzoni MM, Spalleti LA, Andreis RR (1978) Rocas piroclásticas: interpretación y sistemática. Rev Asoc Geol Argent 5:1–58

Vengosh A, Helvaci C, Karamanderesi IH (2002) Geochemical constraints for the origin of thermal waters from Western Turkey. Appl Geochem 17(3):163–183. https://doi.org/10.1016/S0883-2927(01)00062-2

Villalba E (2023) La interacción agua-roca en ambientes hidrológicos asociados a fluidos geotermales. Aplicaciones en calidad de aguas de abastecimiento. PhD Thesis, Facultad de Ciencias Naturales y Museo, Universidad Nacional de La Plata, La Plata, p 171

Villalba E, Carretero SC, Lajoinie MF, Tassi F (2025) Lithogeomorphological factors for wet meadows formation and sustenance in dryland setting in Domuyo mount, Patagonia, Argentina. J South Am Earth Sci 105556. https://doi.org/10.1016/j.jsames.2025.105556

Villalba E, Santucci L, Borzi GE, Pasquini AI, Páez GN, Carol ES (2022) Geothermal Influence on the Hydrochemistry of Surface Streams in Patagonia Neuquina. In: Torres AI, Campodonico VA (eds) Environmental Assessment of Patagonia's Water Resources, Springer International Publishing, Tuscaloosa 57–73 https://doi.org/10.1007/978-3-030-89676-8_3

Villalba E, Tanjal CV, Borzi GE, Páez GN, Carol ES (2020) Geogenic arsenic contamination of wet-meadows associated with a geothermal system in an arid region and its relevance for drinking water. Sci Total Environ 720:137571. https://doi.org/10.1016/j.scitotenv.2020.137571

Wrage J, Tardani D, Reich M, Daniele L, Arancibia G, Cembrano J, Sánchez-Alfaro P, Morata D, Pérez-Moreno R (2017) Geochemistry of thermal waters in the Southern Volcanic Zone, Chile–Implications for structural controls on geothermal fluid composition. Chem Geol 466:545–561. https://doi.org/10.1016/j.chemgeo.2017.07.004

Zaidi FK, Al-Bassam AM, Kassem OM, Alfaifi HJ, Alhumidan SM (2017) Factors influencing the major ion chemistry in the Tihama coastal plain of Southern Saudi arabia: evidences from hydrochemical facies analyses and ionic relationships. Environ Earth Sci 76:1–16. https://doi.org/10.1007/s12665-017-6817-0

Zanettini JCM, Santamaría GR, Leanza H (2001) Provincia Del Neuquén. Hoja Geológica 3772-II, Las Ovejas. Servicio Geológico Minero Argentino, Instituto de Geología y Recursos Minerales